Fizika Nizkikh Temperatur, 2006, v. 32, No. 10, p. 1171–1194

# Carbon «peapods» – a new tunable nanoscale graphitic structure

## (Review Article)

Ilya V. Krive[1,2], Robert I. Shekhter[1], and Mats Jonson[1]

[1]*Department of Physics, Göteborg University, SE-412 96 Göteborg, Sweden*

[2]*B. Verkin Institute for Low Temperature Physics and Engineering, National Academy of Sciences of Ukraine, 47 Lenin Ave., Kharkov 61103, Ukraine*
E-mail:krive@ilt.kharkov.ua

Received December 5, 2005

We consider the ectronic properties of empty single-wall nanotubes (SWNT) and SWNT filled with the fullerenle molecules (carbon «nano-peapod»). The first part of the review (section 2) is devoted mostly to the Luttinger liqued properties of individual metallic SWNT coupled to metallic electrodes or to superconducting leads. The discovery of carbon «nano-peapods» and their elastic, electric and thermal properties are reviewed in the second part of the paper (section 3). We suggest in particularly how fullerene and metallofullerene molecules can be raleased from a «nano-peapod» by a purely electrostatic method.

PACS: **61.48.+c**, **61.46.+w**

**Keywords:** carbon peapod, single-wall carbon nanotube, electrical transport.

Contents



## 1. Introduction

In the context of modern solid state physics interest in carbon-based structures was initially connected to the physics of conducting polymers: in particular to investigations of the physical properties of lightly doped *trans*-polyacetylene (*trans*-$(CH)_x$), which was among the highest-priority research topics in the early 1980s (see, e.g., the review [1]). A number of novel and, for solid state physics, unusual phenomena, such as electron fractionalization, fractional charge, anomalous spin-charge separation, soliton conductivity and others, were reported to be important for describing the conducting properties of lightly doped polyacetylene (see the review [2] and references therein). The joint efforts

of both physicists and chemists during 20 years' of investigating polyacetylene and other conducting polymers culminated in the year 2000, when the Nobel Prize in Chemistry was awarded to A.J. Heeger, A.G. MacDiarmid, and H. Shirakawa for their discovery and development of conducting polymers.

Another area where the interests of physicists and chemists have a strong overlap is related to carbon nanostructures. The birth of this new research area can be attributed to the 1985 discovery [3] of $C_{60}$ (named buckminsterfullerene after the American architect Buckminster Fuller by its discoverers, but also known as «buckyballs»). The synthesis of buckminsterfullerene — a novel molecular form of carbon — was from the very beginning considered to be an outstanding achievement. It triggered an avalanche of publications (see, e.g., the reviews [4,5] and references therein) on the chemical and physical properties of $C_{60}$ as well as other fullerenes and in 1996 R.F. Curl, H.W. Kroto, and R.E. Smalley were awarded by the Nobel Prize in Chemistry for this fundamental discovery.

At first solid state physicists were mostly interested in solid $C_{60}$ (fullerite). Pure fullerites are semiconductors with an energy gap of about 1–2 eV (see, e.g., Ref. 6). When intercalated by alkali metals the compounds $A_3C_{60}$ and $AB_2C_{60}$, (A,B = K, Rb, Cs, Tl) develop a metallic conductivity. At low temperatures these compounds display superconducting properties [7–11] (see also the review [5]). There is a strong correlation between the critical temperature of superconductivity $T_c$ and the lattice spacing $a_0$ in the doped fcc $C_{60}$. The latter depends on the radius of the intercalated atoms and it was found empirically that the critical temperature grows linearly with the increase in lattice spacing ($T_c \propto a_0$) (see the corresponding discussion in Ref. 5). The enhancement of the critical temperature can be qualitatively explained in the BCS theory as a result of the increase in the density of states due to the narrowing of the conduction band following intercalation (see, e.g., Ref. 12). The critical temperatures observed in intercalated fullerites are the highest among superconducting molecular crystals. However, a quantitative theory of superconductivity in these novel materials is still lacking, and even the mechanism of superconductivity in fullerites is under debate [5].

In spite of early optimistic predictions, fullerenes and fullerites, although very interesting objects from the point of view of fundamental science, have still not found vast practical applications. Carbon nanotubes, on the other hand, i.e., microtubules of graphitic carbon, have during the last ten years or so attracted a great deal of interest from experimentalists, theoreticians, and applied scientists because of their considerable potential for applications in, e.g., materials science and electronics. Although vapor-grown carbon filaments have been known and investigated for a long time (see the corresponding brief history in Ref. 13), and the appearance of multi-wall carbon nanotubes (MWNT) in filamentous growth of carbon was reported — using a different language — as early as 1976 by Oberlin, Endo, and Koyama [14], the real surge in the interest in carbon nanotubes started with a paper by Sumio Iijima [15]. In that work, which appeared in 1991 — just after the discovery of fullerenes and at a time when the scientific community was focussed on novel carbon structures; Iijima reported on his discovery of concentric cylindrical multi-wall carbon nanotubes with an outer diameter of 4–30 nm and a length of up to 1 μm in carbonaceous deposits formed in an arc discharge reactor. The electron microscope images obtained in Ref. 15 clearly demonstrate the appearance of concentric cylinders with an inner diameter of about 3 nm and an inter-wall distance of 0.34 nm in the carbon deposit. It was also shown that there are tubes in which the crystal axis of the graphene shell is helically arranged relative to the cylinder axis (they were named *chiral* nanotubes).

In 1993 two experimental groups (one [16] headed by Iijima from NEC Fundamental Research Laboratory in Tsukuba, the other [17] led by Donald Bethune of the IBM Almaden Research Center in San José, California) independently reported the observation of single-wall carbon nanotubes (SWNT). The metals that act as catalysts turn out to be essential for producing SWNTs (see, e.g., Ref. 18). Bethune and his colleagues were experimenting with metal-carbon combinations to generate endohedral species — metallofullerenes. His group and others, inspired by the first successful synthesis [19] of $La@C_{60}$, produced a wide variety of fullerene-based endohedral species with encapsulated La, Ca, Br, Sc, Y, Sr, U, Ti, and other elements (see the review [20]). In experiments with Sc and Er it was shown that a few atoms can be encapsulated in the fullerene cage forming such large metallofullerenes as $Sc_3@C_{82}$ and $Sc_3N@C_{80}$. Then an idea appeared [18] to use transition metal atoms to make endohedral ferromagnetic particles. When vaporized Co was used in an arc discharge reactor, a new graphitic structure — the SWNT — was unexpectedly discovered [17]. Iijima's group chose to use Fe as catalyst element [16]. Soon high-yield production of SWNTs was achieved by laser ablation of graphite [21].

SWNTs are seamless all-carbon nanocylinders. Their diameters range from 0.4 nm to 2–3 nm and the length of these structures can easy reach several micrometers and even millimeters; the longest SWNTs

made so far were 4 cm long [22]. So SWNTs have record-high aspect ratios. Due to their unique mechanical and electrical properties the carbon nanotubes at once attracted the attention of both physicists and engineers. Various potential applications of carbon nanotubes were suggested theoretically and demonstrated in laboratory experiments. Carbon nanotubes are thought to be perfectly fit for use as the basic elements of future nanoelectronics (wires, diodes, transistors, etc.). We will discuss in detail some of the recent progress in understanding the fundamental properties of SWNTs in Section 2 of our review (see also the earlier reviews in Refs. 23–27). One of the most promising applications of nanotubes as field-emitters, first demonstrated in Ref. 28, is already being commercialized in field-emission-based TV displays by Samsung and Motorola.

From the point of view of fundamental physics a metallic SWNT is a realization of a purely 1D conductor, for which Landau's Fermi-liquid theory of conduction electrons is known not to be valid (see, e.g., Ref. 28). Instead, the Luttinger liquid (LL) model [29] (see also the reviews [28,30]) provides the correct low-energy theory of the electronic properties of metallic SWNTs. So far this fundamental property of SWNTs has not been adequately considered in review articles on carbon nanotubes (with the exception of Ref. 31). In subsections 2.2–2.4 the various aspects of this problem and recent developments, including the superconducting properties of SWNTs, are studied.

The next significant achievement in the area of nanoscale graphitic structures was the discovery of carbon «nano-peapods» [32] in 1998 by Brian Smith, Marc Monthioux and David Luzzi. Single-wall nanotubes are hollow cylinders with a nanoscale diameter. Therefore it seems very natural to use them as molecular containers for various substances. Although the idea to fill nanotubes with foreign compounds was obvious to the researchers (see, e.g., Ref. 33) and the attempts to fill MWNTs were successful [34], the first results for SWNTs were obtained only in 1998. Two groups almost simultaneously claimed to have opened and filled single-wall nanotubes. The first foreign material successfully introduced [35] into the interior space of a SWNT was the compound $RuCl_3$, which after heat-treatment under gaseous hydrogen was reduced to metallic Ru. The Oxford team [35] succeeded in deliberately filling SWNTs by using mainly halides as the filling material. Although filling of the SWNT cavity with other materials such as chromium oxide (and other oxide compounds) and even with single elements, *viz*. Ru, Bi, Ag, Au, Pt, and Pd, has been reported in recent years (see, e.g., the review [13] and references therein) it was the discovery of carbon «nano-peapods» — single-wall nanotubes filled with fullerene molecules — that was of most interest to physicists.

The first question concerning peapods that physicists had to answer concerned the status of carbon nano-peapods. Is it a novel graphitic structure with properties that can not simply be reduced to the known properties of SWNTs and fullerene molecules? This problem is considered in subsection 3.2 of Section 3. We will see that carbon peapods do display unique electrical properties. In particular, the $(C_{60}n@(10,10)$ peapod is a system with metallic conductivity both along the nanotube and along the chain of buckyballs [36].

Being a composite system, peapods are easily controlled by acting on their «soft» component — the encapsulated fullerenes. In general, carbon peapods can be thought of as an electromechanical system, where the movable elements — the fullerene molecules — may influence the electrical properties of the peapods. In subsection 3.3 we consider the electrostatics of a carbon nano-peapod coupled to a metallic electrode. Our analysis shows that even an initially neutral $C_{60}$-molecule can be released from the peapod by a purely electrical method.

In the Conclusions section some unsolved problems concerning the physics of carbon nano-peapods and the prospects for using peapods in technological applications are discussed.

## 2. Electronic properties of single-wall nanotubes

It was theoretically predicted [37–40] and then verified in STM experiments [41] that SWNTs, depending on their diameter and helical structure, can demonstrate either metallic or semiconducting behavior. If the chirality of a nanotube is not controlled during the chemical production, something that is not possible at the moment, approximately $1/3$ of all nanotubes display metallic properties. In this review we will consider only metallic nanotubes.

SWNTs are hollow cylinders with a nanometer size diameter. It is physically evident that due to quantization of electron momentum in the compactified direction, the conducting electrons in carbon nanotubes should demonstrate one-dimensional behavior. Besides, in the absence of structural defects their transport along the nanotube shell has to be ballistic. It is known that in the absence of localization a 1D electron system away from half-filling can form either a Luttinger liquid or Peierls-Fröhlich conducting states depending on the effective strength of the electron-electron ($e$–$e$) and electron–phonon ($e$–ph) interactions. As a rule, organic polymers (e.g., *trans*-polyacytelene) and quasi-1D metallic compounds that in principle could be one-dimensional metals, in reality are Peierls insulators

with a charge density wave (CDW), that provides their conducting properties (see, e.g., Ref. 42). So two important questions arise: (i) Why do certain types of SWNTs demonstrate metallic behavior? and (ii) What is the theory of their conducting properties?

### 2.1 Helical structure and electron spectrum

The carbon nanotubes are graphene tubules, so the origin of their specific properties is related to the lattice structure of 2D graphite (graphene) and the «wrapping» procedure, that is the mapping of the graphite sheet onto the cylindrical surface.

The hexagon («honeycomb») lattice structure of 2D graphite shown in Fig. 1 is characterized by the two basis vectors $\mathbf{a}_1$ and $\mathbf{a}_2$ (see e.g., Ref. 23). In a cartesian coordinate system $\mathbf{a}_1 = (a/2)(\sqrt{3}, 1)$ and $\mathbf{a}_2 = (a/2)(\sqrt{3}, -1)$, where $a = \sqrt{3}d_{CC}$ is the lattice spacing and $d_{CC} \simeq 1.4$ Å is the C–C interatomic distance. In Fig. 1 two crystallographically identical points in a honeycomb lattice are connected by a chiral translation vector $\mathbf{C}_h = n_1\mathbf{a}_1 + n_2\mathbf{a}_2$, where $n_{1,2}$ are integers (chiral indices, $0 \le n_2 \le n_1$). Rolling up the 2D graphite sheet into a cylinder corresponds to joining the two lines that are perpendicular to $\mathbf{C}_h$ and goes through the two points where this vector starts and ends. The carbon nanotube is thus specified by the pair of chiral numbers $(n_1, n_2)$ and the cylinder radius is

$$R_{NT} = \frac{|\mathbf{C}_h|}{2\pi} = \frac{a}{2}\sqrt{n_1^2 + n_1 n_2 + n_2^2}\,. \qquad (1)$$

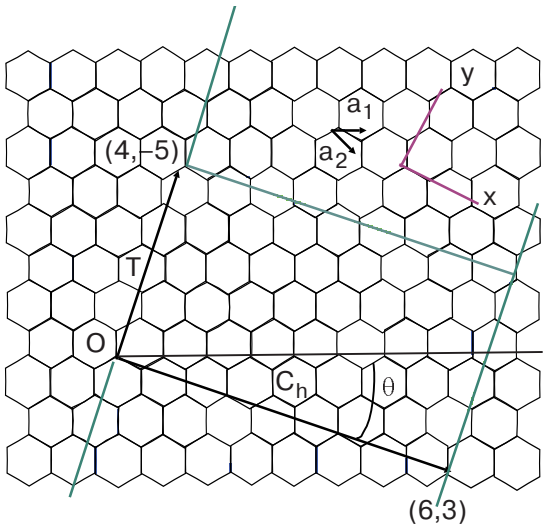


*Fig. 1*. Honeycomb lattice structure of graphene characterized by the two basis vectors $\mathbf{a}_1$ and $\mathbf{a}_2$. A nanotube is formed by rolling up the 2D sheet so that the end of the chiral translation vector $\mathbf{C}_h = n_1\mathbf{a}_1 + n_2\mathbf{a}_2$ at $(n_1, n_2)$ (here (6,3)) meets the origin O. The nanotube translation vector $\mathbf{T}$ is directed along the tube axis. The angle between $\mathbf{a}_1$ (the zigzag direction) and $\mathbf{C}_h$ is the chiral angle $\theta$. This figure is used with permission from S. Mirayama.

For reasons that are evident from Fig. 1 the basis vector $\mathbf{a}_1$ is said to define the *zigzag* direction. If $\mathbf{C}_h$ only has a component along $\mathbf{a}_1$ the corresponding $(n, 0)$-nanotubes are known as «zigzag» nanotubes. The other limiting case corresponds to a translation vector pointing along the bisector of the 60° angle between the two basis vectors, so that $n_1 = n_2 = n$. The resulting $(n,n)$ nanotube is called an «armchair» nanotube. All other types of nanotubes are called «chiral» nanotubes. In these nanotubes the crystal axes of the graphene have a helical arrangement relative to the tube axis.

The graphene is known [23] to be a semimetal in the sense that its Fermi surface collapses to two points (usually labelled $K$ and $K'$) of the Brillouin zone. In the low-energy theory of the graphene electronic structure the effective Hamiltonian, which corresponds to a linearized electron spectrum around these critical points, has the form of a 2D massless Dirac Hamiltonian (see, e.g., Refs. 40,43):

$$H_{\text{eff}} = v_F \boldsymbol{\sigma}\mathbf{k}, \qquad (2)$$

where $\boldsymbol{\sigma}$ are the Pauli matrices and $\mathbf{k}$ is the 2D momentum.

The wave function $\Psi(\mathbf{r})$ of valence electrons has to satisfy periodic boundary conditions along the compactified direction on the cylinder surface. This function can be represented as a product of a crystal (Bloch) function and a slowly varying (envelope) function $\psi(\mathbf{r})$, which satisfies the Schrödinger equation with the Hamiltonian (2). The Bloch function, say for the $K$-point, acquires the phase $\exp(i\mathbf{K}\cdot\mathbf{C}_h)$ ($\mathbf{K}$ is the corresponding crystal momentum) when translated around the tube. Therefore, the envelope function has to satisfy the «twisted» boundary condition $\psi(\mathbf{r} + \mathbf{C}_h) = \exp(-i\mathbf{K}\cdot\mathbf{C}_h)\psi(\mathbf{r})$ to compensate for this phase change. Notice that the twisted boundary conditions can be equivalently expressed in terms of a fictitious magnetic flux $\Phi/\Phi_0 = -\mathbf{K}\cdot\mathbf{C}_h/2\pi$ through the nanotube [43].

The energy spectrum of the Hamiltonian (2) for the boundary condition specified above is [40,43]

$$\varepsilon^{\pm}_{m,\nu}(k) = \pm v_F\sqrt{k^2 + \left(\frac{\hbar}{R_{NT}}\right)^2\left[m - \frac{1}{3}(2n_1 + n_2)\right]^2}, \qquad (3)$$

where $k$ is the electron momentum along the tube axis, $R_{NT}$ is the nanotube radius, Eq. (1), and $m$ is an integer (azimuthal quantum number). According to Eq. (3), the spectrum will be gapless (and the corresponding nanotube metallic) only when [38]

$$2n_1 + n_2 = 3m\,. \qquad (4)$$

Otherwise all electron states have gaps $\Delta E_g$ which scale as $\Delta E_g \propto 1/R_{NT}$. In particular, all armchair SWNTs ($n_1 = n_2$) are metallic wires. This significant prediction [37–39] has been verified experimentally [41]. The low-energy spectra of SWNTs described by the effective Hamiltonian, Eq. (2), are identical for the two critical points $K$ and $K'$. Hence for each metallic SWNT two identical branches of the electron energy spectrum cross the Fermi energy. This double degeneracy can be traced down to the two equivalent 1D sublattices of the honeycomb structure.

From the above analysis it is clear [40] that a real magnetic field parallel to the nanotube axis with noninteger flux $\Phi/\Phi_0$ will induce an energy gap $2\Delta_g$, $\Delta_g = (\hbar v_F/R_{NT})(\Phi/\Phi_0)$, in the electron spectrum of an undoped metallic nanotube (that is at half-filling). The gap $\Delta_g$ for a (10,10) nanotube is of the order of 1 meV for magnetic fields of order a few Tesla. The conductance of SWNTs can therefore be directly controlled by a magnetic field. This interesting theoretical prediction has been reported [44] to have been verified in experiments (see also Ref. 45).

### *2.2. Ballistic transport and Luttinger liquid properties of a metallic SWNT*

It has been known for a long time that a 1D metallic chain of atoms is unstable with respect to a metal-insulator transition caused by a spontaneous lattice distortion. Such a Peierls transition [46] opens up a gap $\Delta_P$ in the electronic energy spectrum exactly at the Fermi level. For a half-filled electron band (in general for commensurate filling) the Peierls state is insulating with an exponentially small conductivity at low temperatures $T << \Delta_P/k_B$. Away from half-filling the Peierls phase transition results in a conducting state (Peierls–Fröhlich state) with a CDW determining the conducting properties of the system at low temperatures (see, e.g., Refs. 42,47). In both cases the density of states (DOS) at the Fermi energy is zero due to the presence of a gap in the energy spectrum of the electrons.

STM experiments [41] unambiguously show that the DOS at the Fermi energy is finite for metallic SWNTs. So, why do SWNTs in contrast to, say, conducting organic polymers like polyacytelene (see, e.g., the review articles [1,2,47]) stay metallic even at low temperatures? There are several physical reasons for this unique behavior. The Peierls transition is a mean-field phenomenon. This is a good approximation when the electron–phonon coupling is strong and the frequency of optical phonons $\omega_{2k_F}$ is low, that is when the lattice vibrations are soft. Even simple estimations of a weak electron–phonon coupling [37] show that the specific nature of the electron spectrum of 2D graphite near the Fermi level leads to a mean-field Peierls transition temperature for carbon nanotubes orders of magnitude below room temperature. Besides, a SWNT have a tubular structure and is not a 1D chain of carbon atoms. The Peierls energy gap was shown [49] to decrease exponentially with an increase of the nanotube radius. For chiral indexes $n \geq 10$ the dependence of $\Delta_P$ on the dimensionless electron–phonon interaction strength becomes analogous to the one in 2D graphite, where the gapless electron spectrum at the Fermi points is known [23] to be stable against a Peierls transition. Finally, the strong (unscreened) Coulomb interaction between electrons in a nanotube requires (see the discussion below) the conduction electrons to be described in terms of a Luttinger liquid (or a 1D Wigner crystal). When the effective electron–phonon coupling is weak, $V_{e-\mathrm{ph}}/\hbar\omega_{2k_F} << 1$, the vibrational modes can be integrated out from the low-energy action and their only effect is to renormalize the LL parameters [48]. So, effects of the electron–phonon interaction on the ground state properties of carbon nanotubes are thought to be negligibly small in general. However, special phonon modes (e.g., the torsional shape fluctuations of the tubular structure [44]) could be a significant factor in the explanation of the temperature dependent resistivity of SWNTs at high temperatures [50].

An isolated armchair SWNT is a half-filled two-band strongly correlated 1D electron system. A gap in the spectrum of charge excitations in this system can be formed due to a Mott transition, which is a metal-insulator phase transition driven by electron correlations. In a Hubbard-like model it has been shown, both for short-ranged electron–electron interactions [51] and long-range Coulomb interactions [52], that the ground state of the half-filled armchair nanotube is indeed a Mott insulator (with an additional gap for spin excitations). The gap in the total charge sector was estimated [52] to be of order 100 K. Notice, however, that *numerical* results obtained in the bozonization approach used in Ref. 52 are questionable, due to their dependence on a cut-off parameter. The cited value for the energy gap should therefore only be considered as an order of magnitude estimate.

The reason why this correlation induced gap has not been observed in experiments measuring the electric current through a nanotube is that a nanotube in contact with metallic leads is shifted away from half-filling by charge transfer between the nanotube and the metal electrodes. Since in current experiments one is normally off half-filling, we will only consider this generic case in what follows.

The above theoretical considerations show that — away from half-filling — SWNTs, which according to

the chiral rule Eq. (4) can be classified as metallic systems, are indeed 1D metals. The first experiments using an individual SWNT [53] or a bundle of high-quality SWNTs [54] demonstrated the ballistic nature of electron transport through a single-wall carbon nanotube. By observing Coulomb blockade phenomena [55,56] the results for the electrical conductance could be interpreted in terms of resonant tunneling through quantized energy levels in the nanotube, and the corresponding electron wave function is delocalized along the entire length of the tube.

The Coulomb interaction between electrons in a 1D quantum wire is intrinsically unscreened (it is screened on the length scale $D >> \lambda_F$ if a bulk metal is located at distance $D$ from the wire). This suggests that Coulomb effects are strong in SWNTs and that they could strongly modify how charge is transported along a quantum wire coupled to source and drain leads.

A long wavelength (low energy) theory of correlated electrons in SWNTs was formulated in Refs. 57 and 58. General considerations suggest that this theory describes a two-channel spin-1/2 Luttinger liquid (see, e.g., Ref. 30). However, the specific features of nanotubes, in particular their tubular structure and the strong (unscreened) Coulomb interaction between electrons, make a detailed study of the different interaction terms motivated [58]. It is physically evident that a poorly screened Coulomb interaction leads to strong *forward* scattering ($\delta k \simeq 0$) of 1D bare electrons. The corresponding scattering amplitude is $V(0) \simeq (2e^2/\kappa) \ln (D/R_{NT})$, where $\kappa \sim 1$ is the dielectric constant. The physical result of strong forward scattering is a strong renormalization of the velocity $v_\rho$ of charge excitations (plasmons), so that $v_\rho >> v_F$. The backscattering terms involve large momentum transfers of order $2k_F$ and hence they are dominated by the short-range part of the Coulomb interaction. Since in a nanotube the conduction electron wave functions have a component that extends around the cylinder, the matrix elements for electron–electron backscattering scale as $1/R_{NT}$ and are small for nanotubes with sufficiently large radii (corresponding to chiral indices $n_{1,2} \geq 10$). A more careful quantitative analysis of scattering vertices induced by the short-range part of the Coulomb interaction shows [58] even an additional numerical suppression. Although these non-LL terms induce gaps in the energy spectra of neutral excitations, the gaps are exponentially small [57,58] and can be safely neglected even at relatively low temperatures. A rough estimation [58] of the corresponding temperature scale gives $T > 0.1$ mK.

The low-energy properties of a SWNT away from half-filling are hence those of a 4-channel Luttinger liquid. The (total) charge sector ($\rho_+$) is the only one that is affected by the Coulomb interaction. The corresponding Hamiltonian takes the form [57,58]

$$H_{\rho_+} = \frac{v_\rho}{2\pi} \int dx \, [g_\rho^{-1} (\partial x \vartheta_{\rho_+})^2 + g_\rho (\partial x \varphi_{\rho_+})^2], \quad (5)$$

where $\vartheta_{\rho_+}$ and $\varphi_{\rho_+}$ are the conjugated bosonic fields of the «total charge» channel, and

$$v_\rho = v_F \sqrt{1 + \frac{8e^2}{\pi \hbar v_F} \ln \frac{D}{R_{NT}}} \quad (6)$$

is the plasmon velocity, while $g_\rho = v_F/v_\rho$ is the LL correlation parameter. All other excitations which correspond to the relative charge channel $\rho_-$ and the total ($\sigma_+$) and relative ($\sigma_-$) spin channels, are described by harmonic fields, as in Eq.(5), but with nonrenormalized velocities ($g = 1$).

The tunneling current into a SWNT can easily be calculated using standard methods of Luttinger liquid theory (see, e.g., Ref. 30). The corresponding problem in a multichannel LL was considered for the first time in Ref. 59. Both the differential and the linear conductance were found to be power-law functions of bias voltage $V$ and temperature $T$,

$$\frac{dJ}{dV} \propto V^\alpha; \quad G(T) \propto T^\alpha \, . \quad (7)$$

Here the exponent $\alpha$ is different for tunneling into the bulk ($\alpha_{\text{bulk}}$) and into the end ($\alpha_{\text{end}}$) of a quantum wire. These two exponents correspond to two different boundary conditions. The «bulk» exponent is calculated for an effectively infinite LL wire and periodic boundary conditions for the plasmonic fields. The «end» exponent corresponds to hard-wall boundary conditions at the nanotube end, where the electron wave function is forced to vanish [60]. In our case [57,58]

$$\alpha_{\text{bulk}} = \frac{1}{8}\left(\frac{1}{g_\rho} + g_\rho - 2\right), \quad \alpha_{\text{end}} = \frac{1}{4}\left(\frac{1}{g_\rho} - 1\right). \quad (8)$$

For strong interactions the electron tunneling to a SWNT is suppressed, which is a manifestation of the Kane–Fisher effect [61]. A theoretical estimation of $g_\rho$ for a micron-length nanotube ($v_F = 8 \cdot 10^5$ m/s for graphene [23]) gives the numerical value $g_\rho \simeq 0.2$ which is in good agreement with experiment [54].

### 2.3. Carbon-based single electron transistor

It has already been known for quite some time [61] that the repulsive electron–electron interaction in one-dimension leads to a dramatic suppression of the charge current through a local potential barrier (see also Ref. 62, where the analogous effect independently was pre-

dicted for a 1D pinned Wigner crystal). The corresponding theoretical problem for an arbitrary interaction can easily be solved analytically for strong and weak barriers by perturbation expansions in the bare tunneling amplitude (weak tunneling) or in the impurity scattering potential (strong tunneling) [63,64]. Although the single-impurity problem in a LL can be solved exactly for an arbitrary barrier [65], universal scaling behavior is pronounced only for the two mentioned limiting cases. Scattering barriers in SWNTs, formed by intrinsic defects, could be strong and in this case they would produce a weak link in the LL wire. For such a situation one can evaluate the nonlinear differential conductance $G(V,T) = dJ/dV$ at finite temperatures in a closed form for arbitrary interaction strengths. When a weak link is formed at the interface between a SWNT and a metallic lead the nonlinear conductance is (see, e.g., Ref. [31]

$$G(V,T) = AT^{\alpha_{\text{end}}} \cosh\left(\frac{eV}{2T}\right)\left|\Gamma\left(\frac{1+\alpha_{\text{end}}}{2} + \frac{ieV}{2\pi T}\right)\right|^2 . \tag{9}$$

Here $\Gamma(z)$ is the gamma function and the prefactor $A$ depends on the bare transparency, which is assumed to be small. For a weak link formed between two identical SWNTs the corresponding nonlinear conductance reads [66]

$$G(V,T) = A'T^{\alpha_{\text{end-end}}} \sinh\left(\frac{eV}{2T}\right) \times$$
$$\times \left|\Gamma\left(\frac{1+\alpha_{\text{end-end}}}{2} + \frac{ieV}{2\pi T}\right)\right|^2 \times$$
$$\times \left\{\frac{1}{2}\coth\left(\frac{eV}{2T}\right) - \frac{1}{\pi}\,\text{Im}\left[\Psi\left(1 + \frac{\alpha_{\text{end-end}}}{2} + \frac{ieV}{2\pi T}\right)\right]\right\}, \tag{10}$$

where $\Psi(z)$ is the digamma function and $\alpha_{\text{end-end}} = 2\alpha_{\text{end}}$. The appearence in Eq. (10) of an exponent twice as large as the one in Eq. (9) is easily explained by the fact that LLs appear on both sides of the barrier. The tunneling rate is therefore determined by the product of two identical power-law functions, each with an exponent $\alpha_{\text{end}}$. According to Eqs. (9) and (10) the differential conductance scaled by $T^{\alpha}$ is a function (for a given interaction strength) of only one variable $eV/T$. This prediction has been confirmed in experiments [66].

An intramolecular junction can be introduced in a SWNT either by creating a pentagon-heptagon defect in the hexagonal carbon tubular structure [66] or by a local mechanical deformation of the uniform nanotube. A SWNT is elastically deformed under a small bending stress and buckles when the mechanical stress exceeds a certain value [67,68]. A sufficiently strong local bending of a SWNT produces a kink-like structure that acts as a scattering barrier for electrons moving along the tube. When two kinks are created not too far from each other, the corresponding doubly buckled SWNT may serve as as an all-carbon room temperature single-electron transistor (SET). The electrical characteristics of such a set was reported for the first time in Ref. 69.

A theory of LL-based SETs was developed in Refs. 70–74. In this chapter we briefly review the novel theoretical predictions made for a SET with electron correlations. The major phenomenon which governs how a standard (semiconducting quantum dot-based) SET works is the Coulomb blockade (CB) of tunneling, which *inter alia* leads to Coulomb blockade oscillations [55] of the current as a function of gate voltage $V_G$. The «orthodox» theory of the Coulomb blockade [55,56] treats electrons as noninteracting quasiparticles and takes into account the long-range part of their Coulomb interaction phenomenologically by introducing the charging energy of the dot

$$E_C(N) = \frac{e^2}{2C}(N - N_G)^2 . \tag{11}$$

This is an electrostatic energy associated with the tunneling of $N - N_0$ electrons onto a dot with $N_0$ electrons and electrical capacitance $C$ in the presence of a gate voltage that controls the parameter $N_G$ (in the CB situation $N_0 < N_G < N_0 + 1$).

There are three different energy scales in the orthodox theory of CB, *viz*. the charging energy $E_C = e^2/2C$, the single electron mean level spacing $\delta$, and the widths of single-particle levels $\Gamma_{l,r}$, ($\Gamma_{\text{tot}} = \Gamma_l + \Gamma_r$) arising due to the finite transparencies of the left ($l$) and right ($r$) barriers which connect the quantum to dot the leads. To have a well-defined number of electrons on the dot, the electron tunneling onto and from the dot should be weak, and therefore $\Gamma_{l,r}$ is taken to be the smallest energy scale in the problem. In the CB regime the temperature has to be much smaller then the charging energy and one may consider two different regimes: (i) the classical Coulomb blockade (high temperature) regime, $\delta << T << E_C$, and (ii) the quantum Coulomb blockade (low temperature) regime, $T << \delta$. The current through the dot is due to single electron tunneling. The current peaks at resonance values of the gate voltage when the CB of single-electron tunneling is lifted. The corresponding charge transfer mechanism is *sequential* electron tunneling onto and out of the quantum dot. At very low temperatures $T << \Gamma_l, \Gamma_r$ this noncoherent mode of electron transport is replaced by resonant, coherent tunneling. Far away

from the resonance points the current is due to direct electron tunneling (cotunneling) through the dot and is strongly suppressed.

The theory of sequential tunneling is based on the master equation approach [55], which describes the time evolution of the probabilities $P_N(t)$ for having $N$ electrons on the dot. The current is calculated using the steady-state probabilities $P_N(\infty)$. The orthodox theory of the classical Coulomb blockade predicts [55,75] a linear temperature dependence of the width of the CB oscillation peaks and temperature independent peak heights.

In the quantum Coulomb blockade regime, $\Gamma_{l,r} << T << \delta$, when only a single electron level on a dot is available for electron transport, the shape of the conductance peaks is (see Eq. (49) in Ref. 76)

$$G_r(\Delta V_G) = \frac{e^2}{\hbar}\,\frac{\Gamma_l\Gamma_r}{\Gamma_l+\Gamma_r}\left(-\frac{\partial}{\partial\varepsilon_G}\,\frac{1}{\exp(\varepsilon_G/T)+1}\right), \tag{12}$$

where $\varepsilon_G \propto \Delta V_G$ is the energy which measures the distance from the resonance point $V_G^{(r)}$; ($\Delta V_G = |V_G - V_G^{(r)}|$). This formula predicts a linear $T$-dependence of the conductance peak width (as in the classical CB regime) and a $1/T$-dependence of the peak heights $G_r(0) \propto T^{-1}$. Equation (12) coincides with the thermally broadened ($T >> \Gamma_{l,r}$) conductance through a Breit–Wigner resonance level.

Coulomb blockade phenomena are pronounced as long as $G_r << G_0 = e^2/\pi\hbar$. This is also the main requirement for the master equation approach to be valid. For a symmetric quantum dot ($\Gamma_l \simeq \Gamma_r$) this assumption is violated at very low temperatures, $T << \Gamma_{l,r}$. In this case transport is through coherent resonant tunneling. The conductance increases with a decrease of temperature and reaches the limit $G_0$ as $T \to 0$.

What novel features do LL correlations add to the picture of single-electron tunneling described above? First of all, the tunneling rates $\Gamma_{l,r}$ being proportional to the tunneling DOS in the «end-coupled» LL, become interaction- and temperature-dependent. As a result the peak conductance acquires a power-law temperature dependence [70] in the whole temperature region $T << E_C$. In addition, new intrinsic energy scales appear. The single-particle level spacing $\Delta_g$ for a finite-length ($L$) LL quantum dot with unscreened Coulomb interactions reads (we use parameters relevant for a SWNT)

$$\Delta_g = \frac{\delta}{g_\rho^2} = \delta + \tilde{E}_c, \quad \tilde{E}_c = \frac{8e^2}{L}\ln\left(\frac{D}{R_{NT}}\right), \tag{13}$$

where $\tilde{E}_c$ defines the corresponding electrostatic (Coulomb) energy. Since $\delta = \pi\hbar v_F/L$ for 1D electrons confined on a quantum dot of length $L$, both terms in Eq. (13) scale as $1/L$. For strong interactions $\Delta_g$ coincides with the Coulomb blockade energy. The new energy scale, which for interacting spinless electrons replaces $\delta$, is the plasmon level spacing $\delta_g = \pi\hbar v_\rho = \delta/g_\rho$ (for strongly interacting electrons $\delta << \delta_g << \Delta_g$). The spin-charge separation in a LL yields two different energy scales for the bosonoc excitations in a LL quantum dot — $\delta_g$ for plasmons and $\delta$ for neutral excitations. The interplay of these energy scales leads to a much more complex picture of Coulomb blockade oscillations [72] than in the case of noninteracting electrons. Besides, the plasmons are bosonic excitations and their statistical properties are significant for determining the occupation probabilities of the energy states in a LL quantum dot [74].

We see that Coulomb blockade phenomena in a SWNT could significantly differ from the standard behavior predicted by the orthodox theory of the CB. The most evident signature of LL effects is the power-law dependence of the conductance on temperature and bias voltage. This dependence originates from the strong energy dependence of the LL tunneling rates in the vicinity of the Fermi energy. For uncorrelated sequential tunneling the resistivities of the left and right LL/quantum dot junctions are effectively added and therefore the temperature dependence of the peak conductance scales as $T^{\alpha_{\rm end}}$ due to the LL correlations (see Eq. (7)) and an additional factor $T^{-1}$, the same as for noninteracting electrons, appears from applying a linear response theory with respect to $eV/T$. In the high-temperature region $\delta_g << T << \Delta_g$ the temperature dependent DOS of the LL dot contributes one more temperature-dependent factor $T^{\alpha_{\rm end}+1}$ to the conductance. In summary, the theory for uncorrelated sequential tunneling (UST) predicts that the peak conductance depends on temperature as follows [70]

$$G_r(T) \propto \begin{cases} T^{\alpha_{\rm end}-1} & \Gamma << T << \delta_g, \\ T^{2\alpha_{\rm end}} & \delta_g << T << \Delta_g. \end{cases} \tag{14}$$

The drama of the situation is that low temperature measurements [69] of $G_r(T)$ for a double-barrier SWNT revealed a different scaling law over a wide temperature interval, since one found that $G_r(T) \propto T^{2\alpha_{\rm end}-1}$.

The theory of uncorrelated sequential tunneling assumes that the bare tunneling amplitudes are small $|t_{l,r}|/\hbar v_F << 1$, and therefore the zero temperature linewidth $\Gamma \propto |t_{l,r}|^2$ is the smallest energy scale in the problem. All calculations in this approach are performed to lowest order in $\Gamma$ (see Refs. 79, 75, 76). It was suggested in Ref. 69 and soon theoretically dem-

onstrated [73,77] that, when processes of higher order in $\Gamma$ are included in the calculation, the new scaling $G_r(T) \propto T^{2\alpha_{\rm end}-1}$ appears for intermediately strong interactions and moderately strong barriers. The corresponding approach was named correlated sequential tunneling (CST). There are serious technical problems with the calculation since all higher order diagrams in $\Gamma$ are intrinsically infrared divergent. These divergencies were avoided in Refs. 73 and 77 by introducing an exponential cutoff factor containing the physical linewidth in the second order diagrams. This linewidth is in its turn determined in a self-consistent manner. Although the procedure is physically reasonable, it introduces an uncontrolled approximation in the problem. Unfortunately, the desired scaling appears in the CST approach as a result of several different contributions and has no clear physical meaning. The existence of a CST regime was confirmed in Ref. 78 by numerical calculations using a quantum Monte Carlo algorithm but has been questioned based on numerical simulations using a functional renormalization group procedure [79]. The problem of finding a physical understanding of the scaling law found in the experiment [69] remains open.

### *2.4. Superconducting properties of carbon nanotubes*

Strong Coulomb correlations as a rule suppress superconductivity and an individual SWNT is not intrinsically superconducting. In a single carbon nanotube the superconducting properties can be induced by the proximity effect of superconducting leads in hybrid S/NT/S or S/NT/N structures (S(N) denotes a superconducting (normal metal) lead). Recently, proximity induced superconductivity was indeed observed in mesoscopic carbon nanotube-based junctions [80–84].

Intrinsic superconductivity in carbon nanotubes has, however, been discovered experimentally [85,86] in ropes containing hundreds of SWNTs at temperatures $T_c \simeq 1$ K. In a thick rope the Coulomb interaction is expected to be partially screened and the electron–phonon interaction may induce superconducting (Cooper) correlations [87,88]. A low-energy (Ginzburg–Landau) theory of superconductivity in bundles of carbon nanotubes was proposed in Ref. 80.

Here we review theoretical models of proximity-induced superconductivity in S/NT/S junctions. The major problem in comparison with the standard description of SNS junctions (see, e.g., Ref. 90 and references therein) is to take into account the strong Coulomb correlations in carbon nanotubes. Depending on the length scale ($L$) of the nanotube that bridges the gap between the two bulk superconductors, two physically different approaches are used to treat this problem. For a long junction, $L >> \xi_0$, where $\xi_0 = \hbar v_F^s/\Delta$ is the superconducting correlation length ($\Delta$ and $v_F^s$ are the energy gap and the Fermi velocity of the superconducting leads), the system is modelled as a superconductor/Luttinger liquid/superconductor (S/LL/S) junction. The short junctions ($L \le \xi_0$) are considered as a superconductor/quantum dot/superconductor (S/QD/S) hybrid system and quantum dot is usually modelled by a single Anderson (or Kondo) impurity.

We start with a long junction. As in the case of normal (nonsuperconducting) leads, the transport properties of an S/LL/S junction strongly depend on the quality of the SN contacts. For adiabatic contacts the Josephson current through the S/LL/S junction is not renormalized by Coulomb interactions. This theorem, which is analogous to «no renormalization» theorems known from similar normal systems (see Ref. 91), was proved for the first time in Ref. 92 (see also 93) by a direct evaluation of the Josephson current through a long perfectly transmitting S/LL /S junction. This result has a clear physical interpretation. In an ideal SNS junction the charge is freely transported through the system due to Andreev reflection of electrons and holes at the SN boundaries. The Andreev boundary conditions for energies $|\varepsilon| << \Delta$; ($\varepsilon$ is counted from the Fermi energy) can be recast [92] in the form of quasiperiodic («twisted») boundary conditions for the right- and left-moving fermions on a ring of circumference $2L$. Then due to translational invariance of the reformulated problem (finding the persistent current in a $S^1$ manifold) the electron–electron interaction does not influence the persistent current of an impurity-free ring (see, e.g., the review [94]).

The Coulomb correlations do affect the supercurrent when normal electron backscattering by local impurities or at SN interfaces is present. SWNTs are known to be ballistic quantum wires and therefore only normal electron reflection at the interfaces between the metallic leads and the Luttinger liquid influences the electrical current. This backscattering process is strongly enhanced by a strong repulsive electron–electron interaction (the Kane–Fisher effect). The bare transparencies of the barriers ($D_{l,r}$) at the interfaces are renormalized by the Coulomb interaction and, as a consequence, the critical Josephson current in a poorly transmitting S/SWNT/S junction is suppressed by the interaction [95]. The corresponding formula for the Josephson current at $T = 0$ reads

$$J = 2J_c^{(0)} R_{\rm int}(L) \sin\varphi, \quad J_c^{(0)} = Dev_F/4L\,, \qquad (15)$$

where $J_c^{(0)}$ is the critical current for a single-channel SNS junction with transparency $D = D_l D_r$ (the addi-

tional factor 2 in Eq. (15) accounts for the two identical conducting channels in a metallic SWNT). The dimensionless interaction-induced renormalization factor $R_{\rm int}(L)$ depends on the geometry of the contact (see Ref. 96). For the standard situation of an end-contacted SWNT $R_{\rm int}$ scales as

$$R_{\rm int} \propto \left(\frac{R_{NT}}{L}\right)^{2\alpha_{\rm end}} << 1. \qquad (16)$$

Here $R_{NT}$ is the nanotube radius and the exponent $\alpha_{\rm end}$ is defined in Eq. (8). Measurements give $\alpha_{\rm end} \simeq 1$, so one can expect the critical current in a long S/SWNT/S junction to approximately scale as $1/L^2$. A detailed theoretical discussion of the properties of the Josephson current through an S/LL/S junction is presented in the review [96].

Until now there has been only one experiment reported [80] where the critical Josephson current was measured in a carbon nanotube-based junction. For the low resistance ($R_0 = 27$ kΩ) «single tube» junction discussed in this work the gap $L \simeq 0.3$ μm between the two superconducting banks (Ta/Au bilayer electrodes) is much smaller than the correlation length of the superconducting electrodes ($T_c \simeq 0.4$ K). So, the theory of Josephson currents in a long S/LL/S junction discussed above can not be applied for explaining the surprising results found in the experiment [80]. In particular, the measured critical current in the «single tube» sample [80] exceeds the Ambegaokar–Baratoff limit for the conventional short SNS junction $i_0 = (\pi/2)(\Delta/eR_N)$, where $R_N$ is the normal junction resistance) by a factor of 40. In Ref. 97 it was claimed that this surprising result can be explained by a Luttinger liquid model of an S/SWNT/S junction. The critical Josephson current calculated in Ref. 97 actually corresponds to the case of a long ($L >> \xi_0$) junction with low transparency ($D << 1$), while in the discussed experiment the fabricated «single tube» junction was short and had a low resistance ($D \simeq 1$). It is worth to stress here that even for noninteracting electrons the critical current in a short junction (the Ambegaokar–Baratoff value) for a given junction transparency is always bigger then the one in a long junction. The Coulomb correlations could only suppress the supercurrent even more. Therefore the surprising result of measurements in Ref. 80 can not be explained by a LL theory with repulsive electron–electron interaction.

Until now, in all experiments with carbon nanotube-based Josephson junctions the fabricated junctions (see, e.g., Refs. 80–84) can roughly be characterized as short. The superconducting properties of a short ($L << \xi_0$) SNS junction are for noninteracting electrons determined by two spin degenerate Andreev bound states [98,99]

$$E_{\pm} = \pm\Delta\sqrt{1 - D\sin^2\left(\frac{\varphi}{2}\right)}. \qquad (17)$$

Here $2\Delta$ is the superconducting gap, $D$ is the junction transparency ($D = 1$ for a perfectly transmitting junction) and $\varphi$ is the superconducting phase difference across the junction. This formula also holds for S/I/N/I/S junctions («I» stands for an insulating layer (barrier) at the SN interface) for nearly transparent barriers $D_l \sim D_r = D_b \simeq 1$ (where $D_b$ is the barrier transparency). In this case the effective transparency $D$ of S/I/N/I/S junction is $D(L) = D_b^2/[D_b^2 + 4(1 - D_b\sin^2(k_{\rm F}L))]$ [90]. According to Eq. (17) the critical current in a multichannel ($N_\perp$ is the number of transverse channels) tunnel ($D << 1$) junction at $T = 0$ is

$$J = \frac{2e}{\hbar}\frac{\partial E_-}{\partial\varphi} = J_c\sin\varphi, \quad J_c = N_\perp D\frac{e\Delta}{2\hbar} \equiv \frac{\pi}{2}\frac{\Delta}{eR_N}, \qquad (18)$$

where $R_N = (\pi\hbar/e^2)(1/N_\perp D)$ is the resistance of the junction in a normal state.

When the barriers at the NS interfaces are thick ($D_b << 1$) the normal part of the junction can be considered to be a quantum dot with a discrete electronic spectrum. Now the expression for the energies of the Andreev bound states corresponding to a resonant level $|\varepsilon_0| << \Delta$ close to the Fermi energy, take the form [100]

$$E_{\pm}^{(QD)} = \pm\sqrt{\Gamma^2\cos^2\frac{\varphi}{2} + \varepsilon_0^2}, \qquad (19)$$

where $\Gamma = D_b\hbar v_F/L << \Delta$, $D_b << 1$ is the width of the resonant electron level. Even in the most favorable situation when the resonant level is exactly at the Fermi energy ($\varepsilon_0 = 0$, $J_c = e\Gamma/2\hbar$) the critical Josephson current is small compared to the maximum critical current of a short fully transparent junction. Notice, however, that the «resonant» Josephson current is determined by the transparency ($D_b << 1$) of only one barrier in a double barrier structure [100]. This is nothing but a manifestation of resonant tunneling in persistent currents [101].

Now we briefly comment on how Coulomb correlations affect the supercurrent in a S/QD/S junction. If the energy level spacing $\delta$ in the quantum dot is much larger then the superconducting gap, $\delta >> \Delta$, only a single energy level in the dot influences the transport properties of the junction. Therefore the dot can be characterized by the level position $-|\epsilon_0|$ counted from the Fermi energy of the leads and the Coulomb interaction $U > 0$. The corresponding Hamiltonian (the Anderson model) reads

$$H_D = \sum_{\sigma=\uparrow,\downarrow} \epsilon_0 \hat{n}_\sigma + U\hat{n}_\uparrow \hat{n}_\downarrow, \qquad (20)$$

where $\hat{n}_\sigma = d_\sigma^\dagger d_\sigma$; ($d_\sigma^\dagger, d_\sigma$ are creation and annihilation operators for electrons in the dot). The dot is coupled to the leads by a standard tunneling Hamiltonian which results in the finite bare width $2\Gamma = \Gamma_l + \Gamma_r$ of the dot energy level. The most interesting physics emerges when $U$ is sufficiently large to make $U + \epsilon_0 > 0$. The energy level of an isolated dot ($\Gamma = 0$) is then singly occupied in the ground state. This singly occupied electron level acts as a spin-1/2 impurity for electrons in the leads and the Kondo effect becomes crucial for determining the low temperature $T < T_K$ ($T_K$ is the Kondo temperature) transport properties of the junction in its normal state. The Kondo temperature in the Anderson model is expressed in terms of the bare model is parameters $U, \Gamma, \epsilon_0$ by the familiar formula [102]

$$T_K = \frac{1}{2} \exp\left\{ \pi \frac{\epsilon_0 (\epsilon_0 + U)}{\Gamma U} \right\}. \qquad (21)$$

It is well known (see, e.g., Ref. 103) that in the Kondo regime $T_K$ is the principle energy scale that determines the low-energy properties of the system, for instance, the temperature dependence of the resistance of a normal metal with dilute magnetic impurities. Superconductivity introduces an additional energy scale, $\Delta$, and the transport properties of S/QD/S junctions strongly depend on the ratio $\Delta/T_K$. For $\Delta << T_K$ superconductivity does not affect the physics of the Kondo effect very much. In the opposite limit ($\Delta >> T_K$) the Kondo effect is completely suppressed. The qualitatively different behavior of a S/QD/S junction in these two limiting cases has a simple physical explanation [103,104].

For a nonsuperconducting N/QD/N junction in the Kondo regime ($T < T_K$) the many-body effects that provide dynamical screening of the S = 1/2 state of the quantum dot by the electrons in the leads, result in the formation of a resonant level of width $T_K$ exactly at the Fermi energy. Electron transport through the junction can effectively be described as electron tunneling through a Breit–Wigner-type resonant level at $E_F$. Correspondingly, the conductance of the system grows with the decrease of temperature and at $T \to 0$ it reaches the quantum unit of conductance $G_0 = 2e^2/h$ as appropriate for a single conducting channel. For superconducting leads with $\Delta << T_K$ the quasiparticle states outside the gap can still provide dynamical screening of the «impurity spin» and the Kondo resonance survives. The effective transparency of the junction deep inside the Kondo regime is perfect, $D = 1$. Therefore the critical Josephson current according to Eqs. (17) and (18) reaches its maximum value $J_c = e\Delta/2\hbar$ for a single channel SNS junction [104].

The Kondo temperature $T_K$, Eq. (21), depends exponentially on the bare level width $\Gamma$. In reality the Kondo effect (with $T_K \sim \Delta$) is observed only in high quality junctions when the normal conductance of the system even in the absence of any Kondo effect (i.e. for an $S = 0$ quantum dot state) is of the order of $e^2/h$. As a rule the opposite limit $T_K << \Delta$ is satisfied for a tunnel junction. Here the Kondo effect is totally suppressed since there are no quasiparticle states that can screen out the spin on the quantum dot. Then the dot acts as an unscreened magnetic impurity.

The influence of spin nonconserving processes on the Josephson current in SIS junctions was first considered by Kulik [105]. It was shown that spin nonconserving tunneling decreases the critical current $J_c \propto |t|^2 - |t_f|^2$ (here $t, t_f$ are the tunneling amplitudes without, $t$, and with, $t_f$, spin flip). According to this dependence the critical current may be even negative. The ground state of the junction with a negative Josephson coupling $\lambda_J = \hbar J_c/2e$ is known as a «π»-junction (the unusual thermodynamical properties of these junctions were first theoretically studied in Ref. 106). The appearance of a negative Josephson coupling is explained physically by the simple fact that electron tunneling through a singly occupied ($S = 1/2$) impurity level flips the electron spin. As a result a Cooper pair is transferred between superconducting banks with opposite sign [107] leading to a negative supercurrent.

A mean field analysis of the magnetic S/QD/S Josephson junction modelled as an Anderson impurity weakly coupled to superconductors showed [108] (see also Ref. 109) that with increased on-site interaction $U$ the critical current is indeed suppressed and eventually changes sign. However, two new intermediate phases (usually labelled as «0′» and «π′») were revealed. In a conventional SIS junction $\varphi = 0$ corresponds to a global minimum of the Josephson energy and $\varphi = \pi$ is an unstable point (global maximum). For a «π»-junction the situation is the opposite. In the intermediate phases both $\varphi = 0$ and $\varphi = \pi$ represent minima. In the «0′»-phase $\varphi = 0$ is a global minimum and $\varphi = \pi$ is a local one and vice-versa for the «π′» phase.

A full numerical (Monte Carlo) analysis of the Josephson current through a magnetic quantum dot was carried out in Ref. 110. There it was shown that only one parameter, $\Delta/T_K$, governs the supercurrent. As expected, the current decreases with an increased value of $\Delta/T_K$. The transition points to the four different quantum phases discussed above, were calculated. In particular it was found that the transition to the «π»-phase is reached at $\Delta/T_K \simeq 11$ and the inter-

mediate «0′» and «π′»-phases exist in the rather wide interval of $\Delta/T_K$-values between 2.8 and 11.

## 3. Fullerenes inside a SWNT (a carbon «nano-peapod»)

The first observation [32] of a carbon peapod, $(C_{60})_n$@SWNT, clearly showed fullerenes inside a SWNT aligned in a regular chain. The properties of carbon peapods can not be simply reduced to the ones characterizing a SWNT and a chain of fullerene molecules. Thus the carbon nano-peapods can be regarded as a new type self-assembled graphitic structure.

### *3.1. Discovery and structural properties of $(C_{60})_n$@ SWNT*

Being theoreticians, the authors can not expertly comment on the experimental procedures and conditions resulting in the discovery of carbon nano-peapods. We will follow the pioneering papers [32, 111] and the reader interested in experimental details should refer to the review Ref. 13.

The single-wall nanotubes used in Refs. 32, 111 were produced by pulsed laser vaporization of graphite in the presence of a metal catalyst. Under the extreme conditions realized in laser ablation of graphite or with the carbon arc discharge method both nanotubes and fullerenes are produced. In the process of carbon nanotube production fullerene molecules are regarded as a contamination and they are removed from the obtained material by acid purification and annealing. During this sequence of processes $C_{60}$-molecules penetrate into the SWNT interior either through the open ends of the nanotubes or through structural defects in the nanotube walls produced at the acid purification stage. In the experiments [32,111] it was directly shown, by using high-resolution transmission electron microscopy (HRTEM), that the buckyballs (closed carbon circles in the HRTEM images) are indeed contained within the SWNT (see Fig. 2). The chain of several fullerenes observed inside a SWNT ($d_{NT} \sim 1.4$ nm) in the cited experiments was rather regular with a period $\sim 1.0$ nm and with a spacing $\sim 0.3$ nm between the carbon shells and the nanotube wall. It was also shown [32] that electron irradiation initiates a dimerization of fullerenes inside a SWNT and sometimes $C_{60}$-molecules coalescence into longer capsules [111,112] thus forming double-wall nanotubes with an inner diameter coinciding with the diameter $\sim 0.7$ nm of a buckyball. Soon after the somewhat accidental discovery of carbon nano-peapods a method for producing this new graphitic structure on a large scale was developed [113]. In this method acid-purified SWNTs are filled

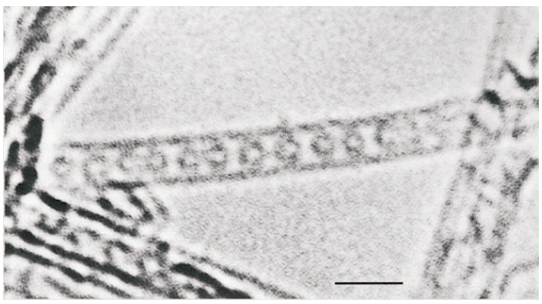

*Fig. 2.* A single-wall carbon nanotube containing a row of closed carbon shells concentric with the tubule axis. The diameter and centre-to-centre spacing of the internal shells are consistent with a chain of $C_{60}$ molecules. The nanotube is surrounded by a vacuum. Scale bar, 2.0 nm. From Ref. 32.

with $C_{60}$-molecules from a gas phase, which is produced by a heat treatment of the SWNTs and the filling material placed in an ampoule sealed under vacuum. It was claimed [113] that the gas-phase filling can result in carbon peapod filling rates of close to 100 %.

The $C_{60}$-molecules inside a SWNT form a 1D van der Waals crystal [111], which is stable up to $\sim 800^\circ$C. Further heating makes the fullerenes coalesce and when the temperature reaches $\sim 1200^\circ$C the carbon peapod is transformed into a double-wall carbon nanotube [112,114].

What is the mechanism of $C_{60}$ encapsulation in SWNTs? As we will see in subsection 2.4 nanotubes with a diameter $d_{NT} \simeq 1.4$ nm (and in particular (10,10) SWNTs), which are abundantly produced by the pulsed laser vaporatization method, are perfectly fitted to encapsulate $C_{60}$ molecules due to the strong gain in van der Waals energy that results from moving a molecule inside such a nanotube. So the first step is to open the SWNT, i.e. to remove the caps at the nanotube ends and/or to produce sufficiently large openings in the nanotube wall. This is achieved by wet chemical etching and is a side effect of the various acid-based purification procedures (see the corresponding discussion in Ref. 13). It is known from experiments [32,112,113] that the optimal temperature for $C_{60}$ encapsulation is about 400 $^\circ$C. It is natural to relate this observation [112] to the fact that the sublimation temperature of solid $C_{60}$ ($T_s \simeq 375$ $^\circ$C, see Ref. 115) is close to the optimal temperature for encapsulation. It was suggested that being in a vapor phase the fullerenes freely fill the empty space inside a nanotube ostensibly via defects. Microscopic processes of fullerene encapsulation were numerically investigated in Ref. 116, where it was shown that the encapsulation of $C_{60}$ molecules through large wall openings is the most likely process of peapod formation. In par-

ticular, the calculations revealed [116] that the probability of successful encapsulation via this process is largest if the velocity of the $C_{60}$ molecules is in the range 80–120 m/s and it almost independent of the launch angle. Therefore the only important quantity for encapsulation is the kinetic energy of the $C_{60}$ molecules. The cited velocity window corresponds to a temperature close to 400 °C, which agrees with the experiments. The authors of Ref. 116 predicted that by increasing the concentration of wall defects the encapsulation efficiency will be improved. Although plausible, the prediction has still not been verified in experiments and the question, whether fullerenes enter the nanotube through the open ends or through the wall defects is open.

Not only $C_{60}$ molecules but metallofullerenes as well can be trapped inside SWNTs. Endotubular metallofullerenes such as $(Gd@C_{82})_n$@SWNT, $(La@C_{82})_n$@SWNT, $(Sm@C_{82})_n$@SWNT and others have already been synthesized and investigated (see the corresponding references in the review paper [13]). The magnetic properties of metallofullerene peapods, although being of a great interest (for instance, for the development of future memory devices), were not studied yet.

### *3.2. Mechanical and electrical properties of carbon nano-peapods*

At first we briefly comment on the elastic properties of carbon peapods.

*3.2.1 Elastic properties*. It is well known (see, e.g., Ref. 23) that the mechanical properties of carbon nanotubes reflect the exceptional stiffness of these structures. Theoretical calculations based on different approximations and calculation schemes (see, e.g., Refs. 117,118 and relevant references therein) predict values for the elastic moduli, which are in agreement with the existing experimental data (notice that so far the experimental uncertainties are quite high). It has also been shown [68] that many mechanical properties calculated from numerical simulations are well reproduced by a continuum shell model for the nanotube with a proper choice of tubular parameters. This statement even holds for nanotube behavior beyond Hook's law [68].

Calculations of the Young's modulus $Y$ of a SWNT predict values of order 1 TPa. Here $Y$ is defined by the standard expression

$$Y = \frac{1}{V_0}\frac{\partial^2 E}{\partial \varepsilon^2}\bigg|_{\varepsilon=0}, \qquad (22)$$

where $\varepsilon$ is the strain, $E(\varepsilon)$ is the strain energy and $V_0 = 2\pi L R_{NT} h$ — $L$ and $R_{NT}$ being the length and radius of the nanotube, while $h$ is the thickness of the nanotube wall — taken to be the same as the interlayer separtion of graphite, $h \simeq 0.34$ nm. Experiments where the Young's modulus for multi-wall nanotubes was measured by analyzing the thermal vibration [119] or with the help of atomic-force microscopy [120] yield the values $Y = (1.8 \pm 1.4)$ TPa and $Y = (1.28 \pm 0.59)$ TPa, respectively. The Poisson ratio $\nu$

$$\frac{\delta R}{R} = -\nu\frac{\delta L}{L}, \qquad (23)$$

calculated in a number of papers (see, e.g., Ref. 118 and references therein) ranges from $\nu \simeq 0.14$ to $\nu \simeq 0.28$. The elastic properties of SWNTs depend weakly on the tube radius, chiral indices and they are very similar to those of a perfect grahite plane (graphene).

One might expect that the filling of a SWNT with fullerene molecules would slightly enhance its stiffness. However, numerical calculations of the Young's modulus and the torsional rigidity of a (10,10) peapod showed [121] that the filled nanotube is slightly (about one percent) softer then an empty tube. The Poisson ratio of the considered carbon nano-peapod was lower by $\sim 5\,\%$ compared with the undoped nanotube. Notice that this result may be specific for the (10,10) peapod. This type of nanotube is almost perfectly fitted to encapsulate $C_{60}$ molecules and the separation of the buckyball shell from the inner surface of the nanotube is very close (but not exactly equal) to the equilibrium distance between $C_{60}$ and graphene. So the composite system $(C_{60})_n$@SWNT is slightly strained compared with the unrolled one. The increase of the total stress energy indicates that the van der Waals interaction between the $C_{60}$-chain and the nanotube inner surface is more significant than the $C_{60}$–$C_{60}$ interaction.

*3.2.2. Density of states and STM spectroscopy*. It is convenient to separate our review of the electrical properties of carbon peapods into two parts. First we will discuss the static electrical properties and this part will be mostly devoted to the problem of how the incorporated fullerenes influence the electronic density of states of SWNTs. Then we will consider the charge transport through an individual peapod and through bundles of $C_{60}$-doped carbon nanotubes.

We saw from the above discussion that the elastic properties of SWNTs are only weakly influenced by $C_{60}$-doping. What is known about electronic properties of nano-peapods? Are they different from those of the constituent parts — a nanotube and a 1D chain of fullerenes?

*Ab initio* numerical calculations [36] based on the so called local density approximation in density func-

tional theory have shown that an armchair (10,10) SWNT filled with $C_{60}$ molecules behaves as a conductor with two different types of charge carriers. The low-energy band structure of this nano-peapod consists of four bands, which cross the Fermi level. Two of the bands are characterized by a linear dispersion with a large Fermi velocity (the same as for any metallic SWNT). The other two bands with much lower Fermi velocity represent the metallic band of the chain of encapsulated fullerenes. So the authors of Refs. 36 claimed that a (10,10) peapod «is a metal with multiple carriers each of which is distributed either on the tube or on the $C_{60}$-chain». This is quite a remarkable prediction since solid $C_{60}$ is a semiconductor with an energy gap of order 1 eV.

This result can be physically explained as follows. Let us consider the lowest unoccupied molecular orbitals (LUMO) and the highest occupied molecular orbitals (HOMO) of a $C_{60}$ molecule. The electronic structure of this molecule is schematically represented in Fig. 3 (see, e.g., Ref. 122). Notice that the energy of the three-fold degenerate LUMO levels ($E_{LUMO} = -4.76$ eV) is quite close to the energy of the Fermi level in metallic SWNTs counted from the vacuum energy (the work function of metallic SWNTs is known to be $W \simeq 5$ eV, see, e.g., Ref. 123 and references therein). This means that one can expect strong mixing of LUMO states with the nanotube conduction states and the bottom of the conduction band of a $C_{60}$ chain inside a (10,10) nanotube should be shifted downward to the nanotube Fermi level.

The structure of electronic states in a (10,10) peapod measured in the experiment of Ref. 124 is in agreement with the cited numerical calculations. In Ref. 124 the electronic charge distribution in bulk samples of SWNTs with a diameter of $(1.37 \pm 0.08)$ nm filled with $C_{60}$'s were measured by electron energy loss spectroscopy. The measurements do demonstrate that there is only a weak van der Waals interaction between the SWNTs and the $C_{60}$ peas, similar to the interaction between $C_{60}$ molecules in solid $C_{60}$. However, the existence of a partially filled conduction band associated with 1D chains of fullerenes inside the carbon nano-peapods was not revealed by the experimental method used in Ref. 124. The excitation spectra of the encapsulated $C_{60}$ peas measured in this work were very similar to the ones in solid $C_{60}$.

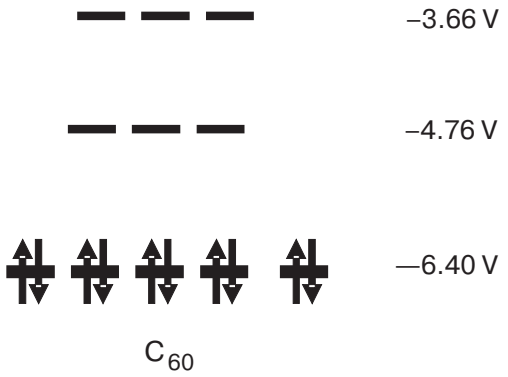


*Fig. 3*. Calculated Kohn–Sham orbital energy patterns of $C_{60}$. Adapted after Ref. 122. Adapted from Ref. 26, with permission from the American Chemical Society 1996.

More detailed information about the electronic density of states in nano-peapods can be obtained by low-temperature scanning tunneling microscopy (STM). Such measurements on carbon peapods were first reported in Ref. 125 (see also Ref. 126, where metallofullerene peapods were investigated by the STM technique). These experiments clearly showed that encapsulated fullerenes do modify the electronic states on the nanotube surface. New features appear in the hybrid system that can not be simply reduced to the properties of the individual subsystems — a carbon nanotube and a fullerene molecule. In the cited experiments all investigated individual nano-peapods appear to be semiconductors. For semiconducting peapods a theory [127] was suggested which succesfully explains many characteristic features of the measured STM spectra. This theory assumes strong mixing of the ball-derived and the tube-derived electronic states and is effectively represented by a long-wavelength Hamiltonian describing the electron dynamics on the tube in the presence of an energy-dependent scattering potential produced by the fullerenes. Since in this review we consider only the properties of metallic nano-peapods, the reader has to refer to the cited papers for detailed information on the STM spectra of semiconducting peapods. Here we also mention Ref. 128 where a theory of electronic states in a semiconducting metallofullerene peapod was suggested. Unlike $C_{60}$-doped nanotubes, where the encapsulated molecules are neutral, metallofullerenes inside a nanotube should be singly positively charged. This results in strong Coulomb effects (localization of electronic states by fullerene charges [128]) in metallofullerene nano-peapods.

It is still not clear either from the experimental or from the theoretical point of view what is the effect of encapsulated neutral $C_{60}$ molecules on the conducting properties of metallic peapods. One can speculate [129] that the strong mixing of LUMO states with the nanotube ungapped propagating states will result in a complicated structure in the electron transmission (with antiresonances, Fano resonances and transmission gaps) through the hybrid systems. On the other hand, symmetry arguments (see the corresponding discussion in Ref. 127) forbid the backscattering of conduction electrons off localized $C_{60}$ or off a periodic

fullerene chainin in a non-chiral SWNT (in particular a (10,10) peapod). So, probably the only effect of $C_{60}$ encapsulation on the conduction properties of metallic non-chiral nano-peapods is the appearence of a narrow conduction band associated with the 1D chain of $C_{60}$ molecules.

*3.2.3. Electrical and thermal transport.* At the present time little is known about the transport properties (both electrical and thermal) of nano-peapods. The few existing experiments, where the electrical conductivity of peapods was measured [113,130,131], used mat-like films («buckypaper») of filled SWNTs and peapod bundles [132] rather then individual peapods. The first measurement of the nano-peapod electrical resistance [113] was carried out on mat-like films of $(Gd@C_{82})_n$@SWNT, $(C_{60})_n$@SWNT and empty SWNTs in a wide temperature interval (5–300 K). The observed temperature dependence of the electrical resistances scales as $\ln R \propto T^{-1/4}$ suggesting that electron transport through the samples is associated with 3D variable range electron hopping. In this conductivity regime the peapod films are characterized by a higher resistance than the samples containing empty nanotubes, which in Ref. 113 was attributed to the scattering of conduction electrons by the electrostatic potential produced by the (presumably charged) fullerenes. The last assumption is reasonable for metallofullerene peapods but seems questionable for $C_{60}$-peapods. The measured high resistance of the samples can in our opinion be caused by the strong disorder (defects) introduced during the synthesis process. An similar temperature dependence of the resistance, suggesting the existence of strong disorder in the system, has been measured [132] for $C_{60}$-peapod bundles bridging the gap between two metal electrodes.

A qualitatively different behavior of the electrical resistance in nano-peapods was reported in Ref. 131. Although the overall temperature dependence of the resistances measured on empty SWNTs and on buckypaper samples with a high (~ 90%) filling fraction of $C_{60}$ was nonmetallic, the peapod samples at low temperatures demonstrated a much lower resistivity compared to the control samples consisting of empty nanotubes. The average diameter of the tubes in the experiment [13] was estimated to be around 1.3 nm. Therefore the formation of an additional conduction band derived from the $C_{60}$ LUMO levels, as predicted [36] for a (10,10) peapod, could be relevant for the condition in this experiment. It was claimed [131] that the increase in the conductivity of $C_{60}$-peapods observed in the experiment «suggests that $C_{60}$ chains provide additional conductive paths for charge carriers».

In the experiment of Ref. 130 it was shown that when doping the peapod system with potassium, the $C_{60}$ molecules inside the SWNT undergo a chemical reaction resulting in the formation of a charged $(C_{60}^{-6})$ covalently bonded one-dimensional polymer chain with metallic conductivity. It is physically evident that the doping of SWNTs and peapods by alkali metal atoms strongly improves the conducting properties of the system since a charge is transferred from the alkali atoms to the nanotube. The unexpected result of Ref. 130 is that in heavily doped peapods the «peas» ($C_{60}$ molecules) are included in the doping process and that a polymerization of $C_{60}$ inside the SWNT is induced.

Now we proceed to commenting on the thermoelectric properties of carbon nano-peapods. As is well known (see, e.g., Ref. 133), there are two transport coefficients — the thermal conductance $K(T)$ and the thermoelectric power $S(T)$ — that characterize thermal transport in conducting systems. These quantities have been repeatedly studied for carbon nanotubes, both theoretically and experimentally. We have already seen in Section 2 that the Luttinger liquid model is the realistic model for the low-energy electronic properties of metallic SWNTs. In an infinite impurity-free LL the thermal conductance associated with charge (plasmons) and spin excitations coincides [134] with that of a 1D channel of noninteracting spin-1/2 fermions. The corresponding formula for $K_F(T)$ is readily derived in the Landauer–Büttiker formalism for transport coefficients (see, e.g., Refs. 135,136). The result is

$$K_F(T) = 2\left(\frac{k_B}{2\pi\hbar T}\right)\int_0^\infty d\varepsilon\,(\varepsilon-\mu)^2\left(-\frac{\partial f_{FD}}{\partial\varepsilon}\right) = \frac{\pi}{3}\frac{k_B T}{\hbar}, \tag{24}$$

where $T$ is the temperature, $\mu >> T$ is the chemical potential, and $f_{FD}$ is the Fermi–Dirac distribution function. The thermal conductance of a perfect, infinite LL wire is a linear function of temperature with a coefficient that depends only on fundamental constants [134]. It is interesting to note here that for a perfect 1D channel the thermal conductance does not depend even on the statistics of the heat carriers [137] (in a LL the heat carriers are bosonic excitations). In the realistic situation when LL wire is coupled to leads of non-interacting electrons the thermal conductance, unlike the electrical conductance, is suppressed even for adiabatic contacts. This is due to a mismatch of the plasmon velocities in the LL wire and in the electron reservoirs [138,139]. The presence of defects (impurities) in the wire additionally suppresses $K(T)$ (see Refs. 134,139, 140) since the heat carriers are backscattered from the local potentials produced by the impurities.

For the thermoelectric power $S(T)$ Luttinger liquid theory predicts a linear temperature dependence at low temperatures with an interaction-dependent coefficient [141,142]. This linear $T$-dependence of $S(T)$ has been observed in experiments on bundles of SWNTs and mat-like samples (see, e.g., Ref. 143) and even some LL effects (in particular the enhancement of the $T$-slope [141]) were observed on SWNT strands containing large number of aligned crystalline ropes [144].

The experimental situation with respect to measurements of the thermal conductivity $\kappa(T)$ in SWNTs is more complex. In metallic nanotubes both electrons and phonons should contribute. The phonon thermal conductivity is given by $\kappa(T) = (1/3)Cv_s l_{\rm ph}$, where $C$ is the specific (per unit volume) heat capacity, $v_s$ is the sound velocity, and $l_{\rm ph}$ is the phonon mean free path. For ballistic transport of 1D phonons the corresponding result for the heat conductance $K_B(T)$,

$$K_B(T) = \frac{k_B}{2\pi\hbar T}\int_0^\infty d\omega\omega^2\left(-\frac{\partial f_{BE}}{\partial\omega}\right) = \frac{\pi}{6}\frac{k_B T}{\hbar}, \qquad (25)$$

($f_{BE}$ is the Bose–Einstein distribution function) is exactly the same as for *spinless* fermions. So the heat conductance of the individual perfect metallic SWNT adiabatically coupled to electron and heat reservoirs is the sum of 3 terms — phonon and spin density excitation contributions, each described by Eq. (25), and a plasmon contribution. In the limit $T \to 0$ the plasmon term is also determined by Eq. (25) while for temperatures $T > \hbar v_\rho / L$, where $v_\rho$ is the velocity of plasmons in a SWNT, and $L$ is the length of the nanotube, it is suppressed roughly by a factor $v_F/v_\rho << 1$ as compared to the phonon and spinon contributions. As a result one can for an ideal situation at low temperatures expect the heat conductance of a metallic SWNT to be $K_{NT}(T) \simeq (\pi/2)(k_B T/\hbar)$.

The theoretical picture described above is, of course, oversimplified for the purpose of comparing with experimental data. In mat-like SWNT samples the presence of numerous defects and tube–tube junctions strongly suppresses electron transport and only phonons contribute to the thermal conductivity. Phonon transport is diffusive up to temperatures $T_m$ when inelastic phonon scattering strongly decreases $l_{\rm ph}$ and the thermal conductivity $\kappa(T)$ starts to drop. In buckypaper samples the scattering of phonons by local potentials produced by numerous tube–tube junctions suppresses the maximum value of $\kappa$ by a few orders of magnitude. So one can only expect to get a high heat conductivity by using individual nanotubes. Numerical calculations [145] for an isolated (10,10) SWNT predict a maximum heat conductivity $\kappa_{\max} \simeq 3{,}7 \cdot 10^4$ W/mK at $T_{\max} \simeq 100$ K comparable to the thermal conductivity of a isolated graphite monolayer (graphene). The measured temperature dependence of the thermal conductivity of individual *multi-wall* carbon nanotubes [146] qualitatively agree with the numerical calculations [145]. However, quantitatively the experimental ($T_{\max} \sim 300$ K, $\kappa_{\max} \simeq 3 \cdot 10^3$ W/mK) and theoretical results are different, which might be attributed to the multi-wall structure of the measured nanotube.

Naively one can expect that the thermal conductivity of a carbon nano-peapod should be higher than for unfilled SWNT. The additional conduction chanels and phonon modes associated with the $C_{60}$ chain inside the nanotube of an ideal individual peapod have to considerably increase $\kappa(T)$ at least at low temperatures. This prediction still has to be verified in experiments with individual nano-peapods. The temperature behavior of the thermal conductivity of SWNTs filled to a high degree by $C_{60}$ as deduced from measurements on buckypaper [131] did not confirm the naive expectations. The measurements [131] indicate little or no contribution of the $C_{60}$ chain to the thermal conductivity.

*3.2.4. A phenomenological theory of carbon nano-peapods*. Electron microscopy images and STM spectroscopy of carbon nano-peapods show that fullerenes inside a carbon nanotube weakly interact with the inner surface of the tube and that in highly filled peapods the $C_{60}$ molecules form a 1D van der Waals crystal. In a series of papers [147–150] a simple semiphenomenological approach to the physics of carbon peapods was suggested. This approach uses van der Waals model potentials for describing the interaction between the various graphitic nano-structures.

One method to obtain graphitic model potentials is based on the Lennard-Jones (LJ) potential (see, e.g., Ref. 151)

$$V_{LJ} = -\frac{A}{r^6} + \frac{B}{r^{12}}. \qquad (26)$$

Here $r$ is the distance between two neutral atoms and the parameters $A, B > 0$ of the attractive and repulsive parts of the LJ potential determine the equilibrium distance $r_0 = (2B/A)^{1/6}$ between the atoms and the well depth $\epsilon = A^2/4B$. The parameters are usually fitted to obtain a good agreement between calculated quantities (such as the cohesive energy and lattice constant of solids) and experimental data. These values are slightly different for the carbon–carbon interaction in different graphitic structures.

The next simplification comes from introducing the continuum approximation, which successfully has been applied, e.g., to calculations of the thermodynamical properties of solid $C_{60}$ (see Ref. 152). In

the continuum model an average surface density of carbon atoms is introduced and the potential between two interacting graphitic structures is averaged over the surface of each entity. The calculations show [147] that in terms of reduced parameters the interaction between various graphitic structures can be represented by an universal curve. The analytic expression for this universal graphitic potential $\Phi(r)$ is [147]

$$\frac{\Phi(r)}{|\Phi(r_0)|} = \frac{5}{3}\left(\frac{3.41}{3.13\tilde{r} + 0.28}\right)^4 - \frac{2}{3}\left(\frac{3.41}{3.13\tilde{r} + 0.28}\right)^{10}. \quad (27)$$

Here $|\Phi(r_0)|$ is the well depth at the equilibrium spacing $r_0$ and the «reduced distance» $\tilde{r} = (r - \rho)/(r_0 - \rho)$. Values of the parameters $|\Phi(r_0)|, \rho$ and $r_0$ for various graphitic structures are listed in Table II of Ref. 147. Notice that the averaging over surfaces of multiatomic interacting structures reduce the exponent in both the attractive $(6 \to 4)$ and the repulsive $(12 \to 10)$ parts of the potential Eq. (27) compared to the LJ potential.

Two quantities are of special interest for us — the binding energy of a $C_{60}$ molecule at a nanotube wall and the entrance potential of a buckyball near the open end of a SWNT. Both quantities were calculated in Ref. 147 and are shown in Figs. 4,*a*,*b*. From Fig. 4,*a* one can see that for a (10,10) nanotube (tube radius $R_{NT} \simeq 0.7$ nm) the binding energy is very close to maximal and that the binding energy rapidly drops with an increase of the tube radius, approaching the binding energy of $C_{60}$ to a graphene sheet for large radii. It should be noticed here, that numerical values for the binding energies calculated using van der Waals potentials [147] strongly differ from the corresponding quantities obtained in *ab initio* calculations [36]. This question was discussed in a special publication [149], where it was argued that the result of Ref. 36 for the binding energy of a $C_{60}$ molecule deep inside a (10,10) nanotube ($\varepsilon_b \simeq 0.5$ eV) is too low. On the other hand, it seems that the semiphenomenological method of model graphitic potentials overestimates the van der Waals cohesive energies (it predicts [147] $\varepsilon_b \simeq 3.26$ eV for a fullerene inside a (10,10) nanotube). A reasonable value for this quantity, which we will use in what follows, is about 2 eV (see, e.g., Ref. 153). The entrance potential, Fig. 4,*b*, is a linear function of distance around the tube end up to distances of approximately the tube radius. After that the potential rapidly saturates.

The fullerene molecules in a fully packed peapod form a one-dimensional structure. In this chain it is reasonable to only consider interactions between nearest-neighbor molecules. The equation of state of a classical 1D gas of particles with short range interactions

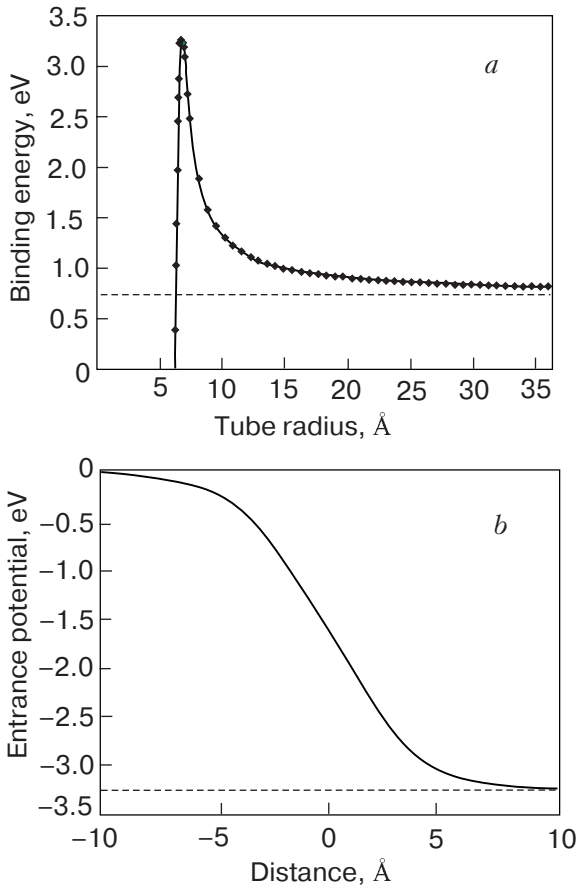


*Fig. 4.* The binding energy of a $C_{60}$ molecule to the inside wall of a single-wall nanotube as a function of tube radius (*a*). The entrance potential for a $C_{60}$ molecule near the open end of a (10,10) single-wall nanotube. From Ref. 26 (*b*).

represented by a pair potential $V(x)$ is exactly known (see, e.g., Ref. 154). The analytical form is

$$n = \frac{\int_0^\infty dx \exp[-\beta(V(x) + xP)]}{\int_0^\infty dx x \exp[-\beta(V(x) + xP)]}, \quad (28)$$

where $n$ is the particle density, $\beta = 1/T$ and $P$ is the pressure. This equation of state was studied in Ref. 150 for the pair potential represented by Eq. (27) and parameters characterizing the $C_{60}$–$C_{60}$ interaction [147]. It was shown that due to the van der Waals interaction between the molecules the pressure at temperatures $T < 10^3$ K is strongly reduced as compared to the pressure of an ideal 1D gas $P_{\text{ideal}} = nk_BT$. The quantum corrections to Eq. (28) due to the zero-point energy were also estimated [150] and it was shown that they can be safely neglected for a $C_{60}$ peapod at $T > 10$ K.

Another analytical approach to the thermodynamics of peapods is to treat fullerenes inside a nanotube as a lattice gas [148]. There is an evident mapping [155] of the lattice gas model to an Ising model. So in the 1D case considered the model is exactly solvable both for canonical (fixed number of molecules) and grand-canonical ensembles (see the corresponding formulae in Ref. 148). Using this approach it was shown [148] that at room temperatures $C_{60}$ molecules inside a nanotube form a single cluster, that is the system is a perfect 1D solid.

### *3.3. Electrostatics of a $C_{60}$-peapod coupled to metallic leads*

Fullerene molecules penetrate a SWNT through the open ends of the tube or through defects (holes) on the tube surface. For stable peapods this process is exothermic and the encapsulation of fullerenes is energetically favorable [36,147,149,153], mostly due to the gain in van der Waals energy. Being inside a tube the fullerenes are confined by a potential that is flat along the tube except in narrow regions of a size of the order of the tube diameter near the tube ends [147]. The potential walls there are high enough to make the peapods absolutely stable at room temperature. For a (10,10) peapod the potential barrier at the tube ends is the highest among all peapods. Barrier heights calculated in different schemes lie in the range 2–4 eV [147,153,156]. Now the important question arises — How can one release fullerene molecules from a peapod?

In metallofullerenes (such as La@$C_{60}$, K@$C_{60}$ and many others) the valence electrons of the metal atom are transferred to the $C_{60}$ shell. This charge transfer is seen in the EPR spectra of the endohedral species (see, e.g., Ref. 18 and references therein). It has also been suggested [158] that when encapsulated in a SWNT the metallofullerenes (e.g., K@$C_{60}$) can be charged if their ionization potential is smaller then the work function of the SWNT. The decapsulation of charged molecules from the interior of a SWNT could then readily be achieved by applying an electric field parallel to the tube axis. A suitable STM-like device with a carbon nano-peapod tip functioning as a nanopipette was theoretically studied in Ref. 157 by molecular dynamics simulations. This work demonstrates the possibility of doing nanolitography by means of a nanopipette based on metallofullerene peapods. Here we suggest to use the electric-field method for decapsulating initially *neutral* $C_{60}$ molecules.

Let us consider a nano-device consisting of a finite length $C_{60}$@(10,10) SWNT peapod placed in the vicinity of a bulk metal electrode (the gap between the SWNT and the bulk electrode is of the order of a few nanotube radii). We [159] show below that when a bias voltage $V_b$ is applied between the tube and the electrode, there is a threshold voltage $V_c$ such that for higher voltages a fullerene inside the tube end will be singly charged. The charged fullerene molecule experiences a strong electrostatic force which for a certain voltage $V_d \geq V_c$ exceeds the van der Waals confinement force and a monoion $C_{60}$ will be driven towards the positively charged electrode. If one neglects the effects of electric-field induced decharging of $C_{60}$ (see the discussion below) at the early stages of decapsulation, the initially neutral fullerene will be realeased from the peapod by a purely electrostatic method.

Our first problem is to calculate the critical voltage $V_c$ for charging an encapsulated buckyball. Physically it is evident that the electric field can not penetrate a semiinfinite metallic tube. This is not the case for a finite-length $L$ tube. Here the potential difference $\Delta V$ between the tube surface and, say, the tube «axis» is finite everywhere. It attains a maximum in the edge regions (of the order of the tube radius $R$) and has tails that decay algebraically, $\sim (R/L)^2$, deep inside the tube. This statement can be easily proven for an empty tube by considering the electrostatic potential $U(z,r)$ produced by a charged metallic tube placed, as in Fig. 5, in the vicinity of a bulk metal electrode

$$U(r,z) = \int_{l}^{l+L} dz' \tau(z') [K(r, z' - z) - K(r, z' + z)] , \quad (29)$$

where $\tau(z')$ is the linear charge density, which has to be determined from the boundary condition

$$U(r = R, z) = V_b, \quad z \in [l, l + L] . \quad (30)$$

Here $R$ is the tube radius, $l$ is the distance from the tube end to the bulk electrode which is assumed to be grounded ($U = 0$), $V_b$ is the bias voltage and $K(r, z' \pm z)$ are the Coulomb kernels for the tube charge and its image in the metal electrode integrated over the azimuthal angle;

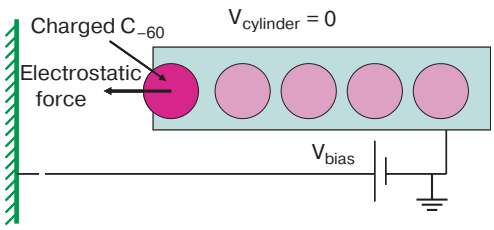


*Fig. 5*. Simple model of a voltage-biased peapod structure close to a metal electrode. The peapod is a chain of $C_{60}$ molecules inside a SWNT with an open end. A large enough bias voltage will make it possible to charge the outermost molecule and expel it from the SWNT (see text).

$$K(r, z' \pm z) = \frac{2}{\pi\sqrt{(r+R)^2 + (z' \pm z)^2}} \times$$

$$\times K\left(2\sqrt{\frac{rR}{(r+R)^2 + (z' \pm z)^2}}\right), \qquad (31)$$

where $K(k)$ is the complete elliptic integral.

For a long tube $L/R >> 1$, $L/l >> 1$ it is reasonable to assume that the charge density $\tau(z)$ is a smooth function of position in the region far from the tube ends $z - l >> R$, $L + l - z >> R$. Then the integral equation (30) can be solved by iterations. In the first approximation the charge density can be taken out of integral Eg. (29) and we easily get for the potential difference $\Delta V_0 = V_b - U(r = 0, z >> R, l)$ the expression

$$\Delta V_0 \simeq \frac{V_b}{4}\left[\left(\frac{R}{z}\right)^2 + \frac{4LzR^2}{(L^2 - z^2)^2}\right] \times$$

$$\times \frac{1}{\ln[4(L-z)z^2/(L+z)R^2]} \qquad (32)$$

which clearly shows that the electric field deep inside a long tube is small.

We will also assume (see also Refs. 157,158) that the charge is homogeneously distributed on the monoion $C_{60}$. Since a fullerene molecule at room temperatures is a swiftly rotating object, this approximation seems quite plausible.

The electrostatic potential for a tube with a singly charged buckyball inside it is in our model determined by the equation

$$U_1(r, z) = \Phi_-(r, z; z_0) + \Phi_+(r, z; z_0) + U(r, z). \qquad (33)$$

Here $\Phi_\pm(r, z; z_0)$ are the standard Coulomb potentials produced by a homogeneously charged sphere placed at position $z_0$ along the tube axis and by its image, located at $-z_0$.

The charge density $\tau(z)$ now has to be determined from an integral equation analogous to Eq. (30), $U_1(r = R) = V_b$.

In order to add an electron to a $C_{60}$ molecule inside a SWNT the electrostatic potential has to compensate for the difference $\delta E$ between the electron binding energy in a metallic SWNT and the analogous energy associated with the $C_{60}$ affinity level. For an isolated buckyball and a SWNT in vacuum this energy difference is $\delta E = W - E_A \simeq 2.3$ eV, where $W \simeq 5$ eV is the work function for a metallic SWNT (see, e.g., Ref. 123 and references therein) and $E_A \simeq 2.7$ eV is the electron affinity for $C_{60}$ (see, e.g., Ref. 122). Notice that the electron affinity for a buckyball molecule is positive and quite large, which makes the $C_{60}$ monoions stable even at high temperatures.

When a buckyball is trapped inside a metallic SWNT the energy of its LUMO (lowest unoccupied molecular orbitals) states can be additionally decreased due to hybridization of the LUMO orbitals with the conduction band states of the nanotube. This effect is more pronounced for small-diameter SWNTs and for stable metallic peapods the hybridization has a maximum for (11,11) SWNTs (see Ref. 153). Numerical calculations using density functional theory in the local density approximation show [36] that in $(C_{60})_n$@(10,10) peapods with $(n >> 1)$ hybridization shifts the conduction band of the otherwise semiconducting 1D $C_{60}$ crystal to the SWNT Fermi level. However, there is experimental evidence that the charge transfer from the SWNT to the fullerene molecules is small [124]. This implies that $C_{60}$ molecules in peapods are neutral and thus $\delta E > 0$. The energy scale of the downward shift of the buckyball LUMO energy levels, which are strongly mixed with the nanotube states, is about 0.3 eV (see Ref. 153). So we can estimate the energy difference in question as $\delta E \simeq 2$ eV.

In order to charge $C_{60}$ inside a nanotube the magnitude of the electrostatic potential energy difference $\Delta U$ between the backyball surface and the SWNT has to be equal to or bigger than $\delta E$. This potential difference can be expressed as $\Delta U \simeq -\alpha(l, z_0)V_b$, where $\alpha < 1$ is a dimensionless coefficient that for a given voltage depends both on the distance $l$ and on the position $z_0$ of the buckyball ($\Delta U < 0$ if $V_b > 0$, see Fig. 5). The threshold voltage for charging is then $V_c = \delta E/e\alpha$. Numerical calculations were performed for a (10,10) peapod of length $L = 30R$ located at distances $l_n = nR$ from the metal electrode, where $n = 2$, 4, 6, 8, and 10. Our results show (see Fig. 6) that for a fixed distance $l$ the numerical factor $\alpha$ rapidly reaches a small constant value for $z_0^{(n)} - l_n >> R$. So in what follows we will put $z_0 = l_n + R_0$ ($R_0$ is the buckyball radius) as the starting stable position of the fullerene molecule. Threshold voltages for the different $l_n$-values considered are $V_c^{(n)} \simeq 16.3$, 19.2, 20.5, 21.2, and 21.8 V. It follows that a bias voltage of about $V_b \sim 20$ V will charge a $C_{60}$ molecule located at the open end of a (10,10) peapod.

The next critical voltage significant for our problem is the threshold voltage $V_d \geq V_c$ for which the singly charged fullerene molecule will be released from the peapod. To estimate this voltage one has to compare the electrostatic force $F(V_e)$ experienced by the charged buckyball at the point $z_0^{(n)}$ with the confinement force which is almost constant and has a maximum $F_W \simeq U_W/2R$ in the region $|z_0^{(n)} - l_n| \leq R$. Here $U_W$ is the height of the confinement potential $U_W \simeq 1.7$ eV for a (10,10) peapod according to DFT

numerical calculations [153]; the semiphenomenological approach based on the van der Waals-like potentials in graphitic nanostructures [147] gives twice as large a value, which seems to be an overestimate.) The critical voltage $V_d$ for fullerene electroemission depends on the distance $l$ between the nanotube and the bulk metal electrode. It coincides with $V_c$ up to a certain distance $l^*$, which has to be found numerically. For $l > l^*$ it is determined by the expression

$$eV_e \simeq \frac{l+R}{2R}\frac{U_W}{1-\alpha(l)} > eV_c. \qquad (34)$$

Our numerical calculations show that at least up to $l = 10R$ a bias voltage of the order of $V_b \simeq 22$ V will be enough to extract fullerene molecules from a (10,10) peapod.

When outside the tube, the $C_{60}$ monoion experiences the strong electric field $E \sim V_b/l$ present in the space between the biased SWNT and the surface of the metal electrode. Therefore there is a finite probability for $C_{60}^-$ to be neutralized by a field emission process. The field emission process dominates when the characteristic time $t_f$ for field induced electron emission from fullerene monoion is shorter than the time $t_c$ it takes for the motion of $C_{60}^-$ inside a gap between biased electrodes. The time $t_f$ can be roughly estimated by the following expression

$$t_f \simeq \omega_t^{-1} D^{-1}(V_b) \simeq \frac{\hbar}{|E_t|}\exp\left(\frac{4\sqrt{2m_e E_A^3}}{3\hbar e V_b l}\right), \qquad (35)$$

where $E_t$ is the energy of the singly occupied LUMO state in $C_{60}^-$ ($E_t \simeq -1.8$ eV, see Ref. 122), $E_A \simeq 2.7$ eV is the electron affinity, which estimates the height of the potential barrier for electron emission from $C_{60}^-$ to vacuum, $m_e$ is the electron mass and $D(V_b)$ in Eq. (35) is the quasiclassical transmission probability for a triangular barrier (see, e.g., Ref. [151]). The transfer time $t_c$ depends on the profile of the electrostatic potential inside the gap region. For motion with constant acceleration $t_c(l) = l\sqrt{2M_0/eV_b}$, where $M_0$ is the buckyball mass. A comparison of the two time scales shows that for $eV_b \simeq 20$ eV electroemission will dominate over monoion charge transport, i.e. $t_f \le t_c$, for small gap sizes up to a few nanometers. This implies that although electron emission hardly could affect the process of fullerene decapsulation, it could be significant for the character of charge transport in devices with a gap of a few nanometers. In particular, one can imagine a scenario where $C_{60}^-$ is decharged while still being in the range of the van der Waals forces from the nanotube. Then a shuttle-like behavior of the fullerene molecule — moving back and forth in the vicinity of the nanotube while being charged and then again discharged — will follow. Notice that direct field emission of electrons from the SWNT is suppressed both due to the higher value of the potential barrier (the work function of a SWNT is about 5 eV) and the Luttinger liquid behavior of the conduction electrons in a SWNT (the last property affects the pre-exponential factor in the Fowler—Nordheim formula, see Ref. 160).

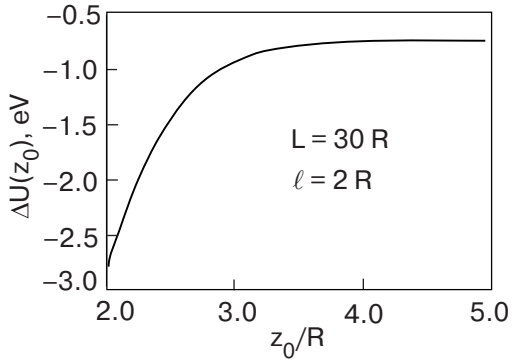


*Fig. 6*. Potential energy difference $\Delta U(z_0)$ as a function of buckyball position $z_0$ for an extra electron on the buckyball surface and on the SWNT calculated using the model system shown in Fig. 5. Here $\Delta U(z_0)$ has been plotted for the case when the electrode in Fig. 5 is biased at $V_b = 10$ V with respect to the grounded nanotube; $L$ is the length and $R$ is the radius of the SWNT, $l$ is the distance between the tube opening and the metal electrode, and $z_0$ is measured from the electrode. An electron is only transferred to the buckyball when $|\Delta U(z_0 = l + R_0)|$, where $R_0 \sim R/2$ is the radius of the $C_{60}$ molecule, becomes equal to the difference $\delta E \sim 2$ eV between the SWNT work function and the $C_{60}$ affinity level energy. Here $(l + R_0)/R \sim 2.5$, so the applied bias in this case is not enough to charge the buckyball; for the parameters used a bias voltage of 16.3 eV is required (see text). Note that $\Delta U(z_0)$ does not go to zero far inside the nanotube. This is because some electrostatic energy can be gained by creating a «hole» in the electron gas on the nanotube surface near a charged buckyball. In agreement with experiment this is, however, not enough to charge a buckyball far inside the SWNT.

## Conclusions

The road from the discovery of fullerenes [3] through the discoveries of carbon nanotubes [15–17] to the synthesis of carbon nano-peapods [32] was not straight. Neither the (empty) single-wall nanotubes (SWNTs) nor the nanotubes filled with $C_{60}$ molecules were deliberately synthesized. Rather these unique nano-structures were by-products in experiments pursuing other goals [13,18]. So it is difficult to predict what new kinds of carbon nanostructures will appear next in this series of remarkable discoveries. Anyway, the 20 year long history of carbon nanostructures

shows that all-carbon materials could be basic elements in the nanotechnology of the 21st century.

So far it is mostly the unfilled carbon nanotubes that have been in the focus of theoretical and experimental studies. The measured characteristics of carbon nano-peapods, which potentially could be an even more unique material than pure SWNTs, are either identical or worse (for instance, with respect to the electrical conductivity) than those of undoped SWNTs. This could be attributed to a still poor quality of the peapods produced at the present time. However, from the point of view of fundamental solid state physics the carbon nano-peapods are indeed unique objects. They allow one to study one-dimensional physics in a real system. In particular, one of the most interesting problem is the superconducting properties of peapods. Both the doped fullerites and ropes of SWNTs are superconductors. Unfortunately the critical temperatures for the superconducting phase transition in these materials are low. There were hopes [161] that carbon nano-peapods could be superconducting even at room temperatures. The theoretical grounds for high-$T_c$ superconductivity in peapods are, however, rather weak. It was suggested that the enhancement of the density of states in the 1D chain of $C_{60}$ molecules could substantially increase the critical temperature. However the Coulomb effects are as strong in carbon nano-peapods as they are in hollow SWNTs (see, e.g., Ref. 162) and Coulomb correlations are known to suppress superconductivity. Unlike unfilled SWNTs, the $C_{60}$ peapods, where the van der Waals forces are «satisfied» internally, are less capable to assemble in ropes and hence screening of the Coulomb interaction in peapods is poor. This problem has not been studied in detail and the expectations to find room temperature superconductivity in nano-peapods (say, metallofullerene peapods) could perhaps be realized in future experiments.

Carbon nano-peapods could be even better field-emitters then empty nanotubes. So their application in STM spectroscopy is very promising. Many other applications of nano-peapods ranging from memory elements («bucky-shuttle», Ref. 158) and 1D wires in nanoelectronics to fuel containers and biocompatible nano-capsules for drugs have been discussed in the literature (see, e.g., Ref. 13,26). At any rate, the «mysterious nano-world that exists inside a carbon nanotube» [163] seems likely to be able to provide unexpected surprises for its explorers also in the future.

This work was supported by the Royal Swedish Academy of Sciences (KVA) and by the Swedish Research Council (VR). The authors thank E. Campbell, D. Fedorets, and E. Pashitskii for numerous fruitful discussions and collaboration. IVK gratefully acknowledges the hospitality of the Department of Physics at Göteborg University.

1. A.J. Heeger, S. Kivelson, J.R. Schrieffer, and W.P. Su, *Rev. Mod. Phys.* **60**, 781 (1988).
2. I.V. Krive and A.S. Rozhavsky, *Usp. Fiz. Nauk* **152**, 33 (1987).
3. H.W. Kroto, J.R. Heath, S.C. O'Brien, R.F. Curl, and R.E. Smalley, *Nature* **318**, 162 (1985).
4. *Clusters and Fullerenes*, V. Kumar, T.P. Martin, and E. Tosatti (eds.), World Scientific, Singapore (1993).
5. A.V. Eletskii and B.M. Smirnov, *Usp. Fiz. Nauk* **169**, 977 (1995).
6. S. Saito and A. Oshiyama, *Phys. Rev. Lett.* **66**, 2637 (1991).
7. A.F. Hebard, M.J. Rosseinsky, R.C. Huddon, D.W. Murphy, S.H. Glarum, T.T.M. Palstra, A.P. Ramirez, and A.R. Kortan, *Nature* **350**, 600 (1991).
8. K. Tanigaki, T.W. Ebessen, S. Saito, J. Mizuki, J.S. Tsai, Y. Kubo, and S. Kuroshima, *Nature* **352**, 222 (1991).
9. M.J. Rosseinsky, A.P. Ramirez, S.H. Glarum, D.W. Murphy, R.C. Huddon, A.F. Hebard, T.T.M. Palstra, A.R. Kortan, S.M. Zahurat, and V. Makhija, *Phys. Rev. Lett.* **66**, 2830 (1991).
10. K. Holezer, O. Klein, S.M. Huang, R.D. Kaner, K.J. Fu, R.L. Wetten, and F. Diederich, *Science* **252**, 1154 (1991).
11. Z. Igbal, R.H. Baughman, B.I. Ramakrishna, S. Khare, N.S. Murphy, H.J. Bornemann, and D.E. Morris, *Science* **254**, 826 (1991).
12. V.M. Loktev and E.A. Pashitskii, *Pis'ma ZhETF* **55**, 465 (1992); V.M. Loktev and E.A. Pashitskii, *Zh. Eksp. Teor. Fiz.* **103**, 594 (1993).
13. M. Monthioux, *Carbon* **40**, 1809 (2002).
14. A. Oberlin, M. Endo, and T. Koyama, *J. Cryst. Growth* **32**, 335 (1976).
15. S. Iijima, *Nature* **354**, 56 (1991).
16. S. Iijima and T. Ichihashi, *Nature* **363**, 603 (1993).
17. D.S. Bethune, C.H. Kiang, M.D. de Vries, G. Gorman, R. Savoy, J. Vazquez, and R. Beyers, *Nature* **363**, 605 (1993).
18. D.S. Bethune, *Physica* **B323**, 90 (2002).
19. J. Heath, S.C. O'Brien, Q. Zhang, Y. Liu, R.F. Curl, H.W. Kroto, F.K. Tittel, and R.E. Smalley, *J. Am. Chem. Soc.* **107**, 7779 (1985).
20. H. Shinohara, *Rep. Prog. Phys.* **63**, 843 (2000).
21. A. Thess, R. Lee, P. Nikolaev, H. Dai, P. Petit, J. Robert, C. Xu, Y.H. Lee, S.G. Kim, A.G. Rinzler, D.T. Colbert, G.E. Scuaeria, D. Tomanek, J.E. Fisher, and R. Smalley, *Science* **273**, 483 (1996).
22. L.X. Zheng, M.J. O'Connell, S.K. Doorn, X.Z. Liao, Y.H. Zhao, E.A. Akhadov, M.A. Hoffbauer, B.J. Roop, Q.X. Jia, R.C. Dye, D.E. Peterson, S.M. Huang, J. Liu, and Y.T. Zhu, *Nature Mater.* **3**, 673 (2004).
23. R. Saito, G. Dresselhaus, and M.S. Dresselhaus, *Physical Properties of Carbon Nanotubes*, Imperial College Press, London (1998).

24. C. Dekker, *Carbon Nanotubes as Molecular Quantum Wires*, *Physics Today* **52**, 5, 22 (1999).
25. P.L. McEuen, *Single-wall Carbon Nanotubes*, *Physics World*, 6 (2000).
26. A.V. Eletskii, *Usp. Fiz. Nauk* **174**, 1191 (2004).
27. Y. Saito, S. Uemura, and K. Hamaguchi, *Jpn. J. Appl. Phys.* **37**, L346 (1998).
28. J. Voit, *Rep. Prog. Phys.* **58**, 977 (1995).
29. F.D.M. Haldane, *J. Phys.* **C14**, 2585 (1981).
30. A.O. Gogolin, A.A. Nersesyan, and A.M. Tsvelik, *Bosonization and Strongly Correlated Systems*, Cambridge University Press (1988).
31. R. Egger et al., in: *Interacting Electrons in Nanostructures*, R. Huang and H. Schoeller (eds.), Springer (2000); *cond-mat/0008008* (2000).
32. B.W. Smith, M. Monthioux, and D.E. Luzzi, *Nature* **396**, 323 (1998).
33. M.S. Dresselhaus, *Nature* **358**, 195 (1993).
34. P.M. Ajayan and S. Iijima, *Nature* **361**, 333 (1993).
35. J. Sloan, J. Hammer, M. Zwiefka-Sibley, and M.L.H. Green, *Chem. Commun*. 347 (1998).
36. S. Okada, S. Saito, and A. Oshiyama, *Phys. Rev. Lett.* **86**, 3835 (2001); A. Oshiyama, S. Okada, and S. Saito, *Physica* **B323**, 21 (2002).
37. J.W. Mintmire, B.I. Dunlop, and C.T. White, *Phys. Rev. Lett*. **68**, 631 (1992).
38. R. Saito, M. Fujita, G. Dresselhaus, and M.S. Dresselhaus, *Appl. Phys. Lett*. **60**, 2204 (1992).
39. N. Hamada, S.-I. Sawada, and A. Oshiyama, *Phys. Rev. Lett*. **68**, 1579 (1992).
40. H. Ajiki and T. Ando, *J. Phys. Soc. Jpn.* **62**, 1255 (1993); T. Ando, H. Matsumura, and T. Nakanishi, *Physica* **B323**, 44 (2002).
41. J.W.G. Wildöer, L.C. Venema, A.G. Rinzler, R.E. Smalley, and C. Deeker, *Nature* **391**, 59 (1998); T.W. Odom, J. Huang, P. Kim, and C.M. Lieber, *Nature* **391**, 62 (1998).
42. G. Grüner, *Density Waves in Solids*, Addison-Wesley Pub. Com. (1994).
43. C.L. Kane and E.J. Mele, *Phys. Rev. Lett.* **78**, 1932 (1997).
44. J.O. Lee, J.R. Kim, J.J. Kim, J. Kim, N. Kim, J.W. Park, and K.H. Yoo, *Solid State Commun.* **115**, 467 (2000).
45. A. Fujiwara, K. Tomiyama, M. Yumura, K. Uchida, and H. Suematsu, *Phys. Rev*. **B60**, 13492 (1999).
46. R.E. Peierls, *Ann. Phys. (Leipzig)* **4**, 121 (1930); *Quantum Theory of Solids*, Oxford U.P., New York (1955).
47. I.V. Krive, A.S. Rozhavsky, and I.O. Kulik, *Fiz. Nizk. Temp*. **12**, 1123 (1986) [*Sov. J. Low Temp. Phys.* **12**, 635 (1986)].
48. J. Voit and H.J. Schulz, *Phys. Rev*. **B36**, 968 (1987); J. Voit and H.J. Schulz, *Phys. Rev*. **B37**, 10068 (1988).
49. R. Saito, M. Fujita, G. Dresselhaus, and M.S. Dresselhaus, *Phys. Rev*. **B46**, 1804 (1992).
50. C.L. Kane, E.J. Mele, R.S. Lee, J.E. Fischer, P. Petit, H. Dai, A. Thess, R.E. Smalley, A.R.M. Verschueren, S.J. Tans, and C. Dekker, *Europhys. Lett*. **41**, 632 (1998).
51. L. Balents and M.P.A. Fisher, *Phys. Rev*. **B55**, R11973 (1997); Yu.A. Krotov, D.-H. Lee, and S.G. Louie, *Phys. Rev. Lett*. **78**, 4245 (1997).
52. H. Yoshioko and A.A. Odintsov, *Phys. Rev. Lett*. **82**, 374 (1999); A.A. Odintsov and H. Yoshioko, *Correlated Electrons in Carbon Nanotubes,* in: *Low Dimensional Systems*, Tobias Brandes (ed.), Springer (2000).
53. S.J. Tans, M.H. Devoret, H. Dai, A. Thess, R.E. Smalley, L.J. Geerligs, and C. Dekker, *Nature* **386**, 474 (1997).
54. M. Bockrath, D.H. Cobden, P.L. McEuen, N.G. Chopra, A. Zettl, A. Thess, and R.E. Smalley, *Science* **275**, 1922 (1997).
55. R.I. Shekhter, *Zh. Eksp. Teor. Fiz*. **63**, 1410 (1972) [*Sov. Phys. JETP* **36**, 747 (1972)]; I.O. Kulik and R.I. Shekhter, *Zh. Eksp. Teor. Fiz*. **68**, 623 (1975) [*Sov. Phys. JETP* **41**, 308 (1975)].
56. H. Grabert and M.H. Devoret (eds.), *Single Charge Tunneling: Coulomb Blockade Phenomena in Nanostructures*, Plenum, New York (1992).
57. C. Kane, L. Balents, and M.P.A. Fisher, *Phys. Rev. Lett.* **79**, 5086 (1997).
58. R. Egger and A.O. Gogolin, *Phys. Rev. Lett*. **79**, 5082 (1997).
59. K.A. Matveev and L.I. Glazman, *Phys. Rev. Lett.* **70**, 990 (1993).
60. M. Fabrizio and A.O. Gogolin, *Phys. Rev*. **B51**, 17827 (1995).
61. C.L. Kane and M.P.A. Fisher, *Phys. Rev. Lett*. **68**, 1220 (1992).
62. L.I. Glazman, I.M. Ruzin, and B.I. Shklovskii, *Phys. Rev*. **B45**, 8454 (1992).
63. C.L. Kane and M.P.A. Fisher, *Phys. Rev*. **B46**, 15233 (1992).
64. A. Furusaki and N. Nagaosa, *Phys. Rev*. **B47**, 4631 (1993).
65. P. Fendley, A.W.W. Ludvig, and H. Saleur, *Phys. Rev. Lett*. **74**, 3005 (1995); P. Fendley, A.W.W. Ludvig, and H. Saleur, *Phys. Rev*. **B52**, 8934 (1995); H. Saleur, *Lectures on Nonperturbative Field Theory and Quantum Impurity Problems*, Les Houches Session LXIX, Springer (1999).
66. Z. Yao, H.W.Ch. Postma, L. Balents, and C. Dekker, *Nature* **402**, 273 (1999).
67. S. Iijima, C.J. Brabec, A. Maiti, and J. Bernholc, *J. Chem. Phys*. **104**, 2089 (1996).
68. B.I. Yakobson, C.J. Brabec, and J. Bernholc, *Phys. Rev. Lett*. **76**, 2511 (1996).
69. H.W.Ch. Postma, T. Teepen, Z. Yao, M. Grifoni, and C. Dekker, *Science* **293**, 76 (2001).
70. A. Furusaki, *Phys. Rev*. **B57**, 7141 (1998).
71. A. Braggio, M. Grifoni, M. Sassetti, and F. Napoli, *Europhys. Lett*. **50**, 236 (2000).
72. A. Braggio, M. Sassetti, and B. Kramer, *Phys. Rev. Lett*. **87**, 146802 (2001).

73. M. Thorwart, M. Grifoni, G. Cuniberti, H.W.Ch. Postma, and C. Dekker, *Phys. Rev. Lett*. **89**, 196402 (2002).
74. J.U. Kim, I.V. Krive, and J. Kinaret, *Phys. Rev. Lett*. **90**, 176401 (2004).
75. L.I. Glazman and R.I. Shekhter, *J. Phys.: Cond. Matter* **1**, 5811 (1986).
76. C.W.J. Beenakker, *Phys. Rev.* **B44**, 1646 (1991).
77. M. Thorwart, R. Egger, and M. Grifoni, *Phys. Rev*. **B72**, 03550 (2005).
78. S. Hügle and R. Egger, *Europhys. Lett*. **66**, 565 (2004).
79. V. Meden, T. Enss, S. Andergassen, W. Metzner, and K. Schönhammer, *Phys. Rev.* **B71**, 04102 (2005); T. Enss, V. Meden, S. Andergassen, X. Barnabe-Theriault, W. Metzner, and K. Schönhammer, *Phys. Rev*. **B71**, 155401 (2005).
80. A.Yu. Kasumov, R. Deblock, M. Kociak, B. Reulet, H. Bouchiat, I.I. Khodos, Yu.B. Gorbatov, V.T. Volkov, C. Journet, and M. Burghard, *Science* **284**, 1508 (1999).
81. A.F. Morpurgo, J. Kong, C.M. Marcus, and H. Dai, *Science* **286**, 263 (1999).
82. M.R. Buitelaar, T. Nussbaumer, and C. Schönenberger, *Phys. Rev. Lett*. **89**, 256801 (2002).
83. M.R. Buitelaar, W. Belzig, T. Nussbaumer, B. Babic, C. Bruder, and C. Schönenberger, *Phys. Rev. Lett*. **91**, 057005 (2003).
84. M.R. Gräber, T. Nussbaumer, W. Belzig, and C. Schönenberger, *Nanotechnology* **15**, S479 (2004).
85. M. Kociak, A.Y. Kasumov, S. Gueron, B. Reulet, I.I. Khodos, Y.B. Gorbatov, V.T. Volkov, L. Vaccarini, and H. Bouchiat, *Phys. Rev. Lett*. **86**, 2416 (2001).
86. Z.K. Tang, L.Y. Zhang, N. Wang, X.X. Zhang, G.H. Wen, G.D. Li, J.N. Wang, C.T. Chan, and P. Sheng, *Science* **292**, 2462 (2001).
87. J. Gonzalez, *Phys. Rev. Lett*. **88**, 076403 (2002); J. Gonzalez, *Phys. Rev*. **B67**, 014528 (2003).
88. A. De Martino and R. Egger, *Phys. Rev*. **B67**, 235418 (2003).
89. A. De Martino and R. Egger, *Phys. Rev*. **B70**, 014508 (2004).
90. P. Samuelsson, J. Lantz, V.S. Shumeiko, and G. Wendin, *Phys. Rev*. **B62**, 1319 (2000).
91. D.L. Maslov and M. Stone, *Phys. Rev*. **B52**, R5539 (1995); V.V. Ponomarenko, *ibid*. **B52**, R8666 (1995); I. Safi and H.J. Schulz, *ibid*. **B52**, R17040 (1995).
92. D.L. Maslov, M. Stone, P.M. Goldbart, and D. Loss, *Phys. Rev*. **B53**, 1548 (1996).
93. I. Affleck, J.-S. Caux, and A.M. Zagoskin, *Phys. Rev*. **B62**, 1433 (2000).
94. A.A. Zvyagin and I.V. Krive, *Fiz. Nizk. Temp*. **21**, 687 (1995) [*Low Temp. Phys*. **21**, 533 (1995)].
95. R. Fazio, F.W.J. Hekking, and A.A. Odintsov, *Phys. Rev. Lett*. **74**, 1843 (1995).
96. I.V. Krive, S.I. Kulinich, R.I. Shekhter, and M. Jonson, *Fiz. Nizk. Temp*. **30**, 738 (2004) [*Low Temp. Phys*. **30**, 554 (2004)].
97. J. Gonzalez, *Phys. Rev. Lett*. **87**, 136401 (2001); J. Gonzalez, *J. Phys.*: *Condens Matter* **15**, S2473 (2003).
98. A. Furusaki and M. Tsukuda, *Physica* **B165–166**, 967 (1990); S.K. Kuplevakhskii and I.I. Fal'ko, *Fiz. Nizk. Temp.* **17**, 961 (1991) [*Sov. J. Low Temp. Phys*. **17**, 501 (1991)].
99. C.W.J. Beenaker and H. van Houten, *Phys. Rev. Lett*. **66**, 3056 (1991).
100. G. Wendin and V.S. Shumeiko, *Superlattices Microstruct*. **4**, 569 (1996).
101. P. Sandström and I.V. Krive, *Phys. Rev*. **B56**, 9255 (1997).
102. F.D.M. Haldane, *Phys. Rev. Lett*. **40**, 416 (1978).
103. L. Kouwenhoven and L. Glazman, *Physics World* **1**, 33 (2001).
104. L.I. Glazman and K.A. Matveev, *Pis'ma Zh. Eksp. Teor. Fiz*. **49**, 570 (1989) [*JETP Lett*. **49**, 659 (1989)].
105. I.O. Kulik, *Sov. Phys. JETP* **22**, 841 (1966).
106. L.N. Bulaevskii, V.V. Kuzii, and A.A. Sobyanin, *JETP Lett*. **25**, 290 (1977).
107. B.I. Spivak and S.A. Kivelson, *Phys. Rev*. **B43**, 3740 (1991).
108. A.V. Rozhkov and D.P. Arovas, *Phys. Rev. Lett*. **82**, 2788 (1999).
109. E. Vecino, A. Martin-Rodero, and A. Levy Yeyati, *Phys. Rev*. **B68**, 035105 (2003).
110. F. Siano and R. Egger, *Phys. Rev. Lett*. **93**, 047002 (2004).
111. B.W. Smith, M. Monthioux, and D.E. Luzzi, *Chem. Phys. Lett*. **315**, 31 (1999).
112. B.W. Smith and D.E. Luzzi, *Chem. Phys. Lett*. **321**, 169 (2000).
113. K. Hirahara, K. Suenaga, S. Bandow, H. Kato, T. Okazaki, H. Shinohara, and S. Iijima, *Phys. Rev. Lett*. **85**, 5384 (2000).
114. S. Bandow, M. Takizawa, K. Hirahara, M. Yudasaka, and S. Iijima, *Chem. Phys. Lett.* **337**, 48 (2001).
115. C.K. Mathews, M. Sai Baba, T.S. Lakshmi Narasimhan, R. Balasubramanian, N. Sivaraman, T.G. Srinivasan, and P.R. Vasudeva Rao, *J. Phys. Chem*. **96**, 3566 (1992).
116. S. Berber, Y.-K. Kwon, and D. Tomanek, *Phys. Rev. Lett*. **88**, 185502 (2002).
117. E. Hernandez, C. Goze, P. Bernier, and A. Rubio, *Phys. Rev. Lett*. **80**, 4502 (1998).
118. D. Sanchez-Portal, E. Artacho, and J.M. Soler, *Phys. Rev*. **B59**, 12678 (1999).
119. M.M.J. Treacy, T.W. Ebbesen, and J.M. Gibson, *Nature* **381**, 678 (1996).
120. E.W. Wong, P.E. Sheedan, and C.M. Lieber, *Science* **277**, 1971 (1977).
121. A.A. Farajian and M. Mikami, *J. Phys.*: *Condens. Matter* **13**, 8049 (2001).
122. W.H. Green, Jr., S.M. Gorun, G. Fitzgerald, P.W. Fowler, A. Ceulemans, and B.C. Titeca, *J. Phys. Chem*. **100**, 14892 (1996).

123. G. Zhou, W. Duan, and B. Gu, *Phys. Rev. Lett*. **87**, 095504 (2001); G. Zhou and Y. Kawazoe, *Phys. Rev*. **B65**, 155422 (2002).
124. X. Liu, T. Pichler, M. Knupfer, M.S. Golden, J. Fink, H. Kataura, Y. Achiba, K. Hirahara, and S. Iijima, *Phys. Rev*. **B65**, 045419 (2002).
125. D.J. Hornbaker, S.-J. Kahng, S. Misra, B.W. Smith, A.T. Johnson, E.J. Mele, D.J. Luzzi, and A. Yazdani, *Science* **295**, 828 (2002).
126. J. Lee, H. Kim, S.-J. Kahng, G. Kim, Y.-W. Son, J. Ihm, H. Kato, Z.W. Wang, T. Okazaki, H. Shinohara, and Y. Kuk, *Nature* **415**, 1005 (2002).
127. C.L. Kane, E.J. Mele, A.T. Johnson, D.E. Luzzi, B.W. Smith, D.J. Hornbaker, and A. Yazdani, *Phys. Rev*. **B66**, 235423 (2002).
128. J. Gonzalez and F. Guinea, *Phys. Rev*. **B71**, 193409 (2005).
129. D.H. Kim, H.-S. Kim, and K.J. Chang, *Phys. Rev*. **B64**, 115409 (2001).
130. T. Pichler, H. Kuzmany, H. Kataura, and Y. Achiba, *Phys. Rev. Lett*. **87**, 267401 (2001).
131. J. Vavro, M.C. Llaguno, B.C. Satishkumar, D.E. Luzzi, and J.E. Fischer, *Appl. Phys. Lett*. **80**, 1450 (2002).
132. H. Hongo, F. Nihey, M. Yudasaka, T. Ichihashi, and S. Iijima, *Physica* **B323**, 244 (2002).
133. J.M. Ziman, *Principles of the Theory of Solids*, Cambridge Univ. Press, Cambridge (1986).
134. C.L. Kane and M.P.A. Fisher, *Phys. Rev. Lett.* **76**, 3192 (1996).
135. E.N. Bogachek, I.O. Kulik, and A.G. Shkorbatov, *Fiz. Nizk. Temp*. **11**, 1189 (1985) [*Sov. J. Low Temp. Phys*. **11**, 656 (1985)].
136. U. Sivan and Y. Imry, *Phys. Rev*. **B33**, 551 (1986).
137. I.V. Krive and E. Mucciolo, *Phys. Rev*. **B60**, 1429 (1999).
138. R. Fazio, F.W.J. Hekking, and D.E. Khmelnitskii, *Phys. Rev. Lett*. **80**, 5611 (1988).
139. I.V. Krive, *Fiz. Nizk. Temp*. **24**, 458 (1998) [*Low Temp. Phys*. **24**, 377 (1998)].
140. I.V. Krive, *Phys. Rev*. **B59**, 12338 (1999).
141. I.V. Krive, E.N. Bogachek, A.G. Scherbakov, and U. Landman, *Phys. Rev*. **B63**, 113101 (2001).
142. I.V. Krive, I.A. Romanovsky, E.N. Bogachek, A.G. Scherbakov, and U. Landman, *Fiz. Nizk. Temp*. **27**, 1110 (2001) [*Low Temp. Phys*. **27**, 821 (2001)]; I.A. Romanovsky, I.V. Krive, E.N. Bogachek, and U. Landman, *Phys. Rev*. **B65**, 075115 (2002).
143. J. Hone, E.I. Muno, A. Mizel, M.L. Cohen, A. Zettle, A.G. Rinzler, and R.E. Smalley, *Phys. Rev. Lett.* **80**, 1042 (1998); G.U. Sumanasekera, G.D. Mahan, and P.C. Eklund, *Phys. Rev*. **B65**, 205410 (2002).
144. W.J. Kong, L. Lu, H.W. Zhu, B.Q. Wei and D.H. Wu, *J. Phys.: Condens.Matter* **17**, 1923 (2005).
145. S. Berber, Y.-K. Kwon, and D. Tomanek, *Phys. Rev. Lett*. **84**, 4613 (2000).
146. P. Kim, L. Shi, A. Majumdar, and P.L. McEuen, *Phys. Rev. Lett*. **87**, 210522 (2001); *Physica* **B323**, 67 (2002).
147. L.A. Girifalco, M. Hodak, and R.S. Lee, *Phys. Rev*. **B62**, 13104 (2000).
148. M. Hodak and L.A. Girifalco, *Phys. Rev*. **B64**, 035407 (2001).
149. L.A. Girifalco and M. Hodak, *Phys. Rev*. **B65**, 125404 (2002).
150. M.M. Calbi, S.M. Gatica, and M.W. Cole, *Phys. Rev*. **B67**, 205417 (2003).
151. L.D. Landau and E.M. Lifshitz, *Quantum Mechanics*, Pergamon Press, Oxford (1981).
152. L.A. Girifalco, *Phys. Rev*. **B52**, 9910 (1995).
153. S. Okada, M. Otani, and A. Oshiyama, *Phys. Rev*. **B67**, 205411 (2003).
154. R.P. Feynman, *Statistical Mechanics*: *A set of Lectures* (Frontiers in Physics Series), Addison-Wesley Pub. Com. (1972), p.117.
155. C.N. Young and T.D. Lee, *Phys. Rev*. **87**, 410 (1952).
156. H. Ulbricht, G. Moos, and T. Hertel, *Phys. Rev. Lett*. **90**, 095501 (2003).
157. H.J. Hwang, K.R. Byun, and J.W. Kang, *Physica* **E23**, 208 (2004).
158. Y.K. Kwon, D. Tomanek, and S. Iijima, *Phys. Rev. Lett*. **82**, 1470 (1999).
159. The original results of this section were obtained by the authors in collaboration with E. Pashitskii and D. Fedorets.
160. A.O. Gogolin and A. Komnik, *Phys. Rev. Lett*. **87**, 256806 (2001).
161. R.F. Service, *Science* **292**, 45 (2001).
162. W. Que, *Phys. Rev*. **B66**, 193405 (2002); W. Que, *ibid*. **B67**, 129901 (2003).
163. S. Iijima, *Physica* **B323**, 1 (2002).